

Article

FSH blockade improves cognition in mice with Alzheimer's disease

<https://doi.org/10.1038/s41586-022-04463-0>

Received: 16 July 2020

Accepted: 25 January 2022

Published online: 2 March 2022

 Check for updates

Jing Xiong^{1,2,9}, Seong Su Kang^{1,9}, Zhihao Wang¹, Xia Liu¹, Tan-Chun Kuo³, Funda Korkmaz³, Ashley Padilla³, Sari Miyashita³, Pokman Chan⁴, Zhaohui Zhang², Pavel Katsel⁵, Jocoll Burgess^{3,5}, Anisa Gumerova³, Ksenilia Levleva³, Damini Sant³, Shan-Ping Yu⁶, Valeria Muradova³, Tal Frolinger³, Daria Lizneva³, Jameel Iqbal³, Ki A. Goosens^{3,5}, Sakshi Gera³, Clifford J. Rosen⁷, Vahram Haroutunian⁵, Vitaly Ryu³, Tony Yuen³, Mone Zaidi^{3,8} & Keqiang Ye^{1,8,✉}

Alzheimer's disease has a higher incidence in older women, with a spike in cognitive decline that tracks with visceral adiposity, dysregulated energy homeostasis and bone loss during the menopausal transition^{1,2}. Inhibiting the action of follicle-stimulating hormone (FSH) reduces body fat, enhances thermogenesis, increases bone mass and lowers serum cholesterol in mice^{3–7}. Here we show that FSH acts directly on hippocampal and cortical neurons to accelerate amyloid-β and Tau deposition and impair cognition in mice displaying features of Alzheimer's disease. Blocking FSH action in these mice abrogates the Alzheimer's disease-like phenotype by inhibiting the neuronal C/EBPβ-δ-secretase pathway. These data not only suggest a causal role for rising serum FSH levels in the exaggerated Alzheimer's disease pathophysiology during menopause, but also reveal an opportunity for treating Alzheimer's disease, obesity, osteoporosis and dyslipidaemia with a single FSH-blocking agent.

Alzheimer's disease (AD) is a neurodegenerative disorder of the aging population that shows a higher incidence in women after the menopause⁸. With the paucity of disease-modifying agents, AD poses a major global health crisis, resulting in progressive dementia, profound disability and impaired quality of life. Neuropathological hallmarks include aggregated amyloid-β (Aβ) peptides and Tau proteins and chronic inflammation. Constituting around 70% of individuals with AD, women have a greater life-time risk for AD than men, and display approximately a threefold higher rate of disease progression with a broader spectrum of cognitive symptoms^{9,10}. The cause of this gender difference is unclear. A role for post-menopausal reductions in serum oestrogen remains controversial; improvement¹¹, no change^{12,13} and worsening¹⁴ of cognition have been shown after oestrogen-replacement therapy. By contrast, high serum levels of pituitary gonadotropins, including FSH, are strongly associated with the onset of AD and have therefore been suggested as possible mediators^{15,16}. There is also a period in a woman's life before the last menstrual period when oestrogen levels are relatively unperturbed, while serum FSH is rising sharply¹⁷. During this perimenopausal phase, which normally occurs between the ages of 42 and 52 years¹⁷, there is a transient decline in cognition, prominently verbal memory^{18–20}. This striking oestrogen-independent correlate prompted us to investigate whether FSH has a causal role in AD pathogenesis, and whether blocking FSH action may provide a means of ameliorating AD.

FSH-Ab prevents the AD phenotype

Our anti-FSHβ antibody (FSH-Ab) targets a 13-amino-acid mouse FSHβ sequence, LVYKDPARPNTQK, blocks FSH action on bone cells and adipocytes and, in doing so, increases bone mass, decreases body fat and elevates energy expenditure in mice^{5,6,21}. Here we show that FSH-Ab inhibits plaque and neurofibrillary tangle formation and reverses cognitive decline in ovariectomized 3xTg-AD (3xTg) mice (Fig. 1). These mice have a human transgene with mutated APP^{K670N/M671L} and MAPT^{P301L}, and a *Psen1*^{M146V} knockin mutation, and display associative learning deficits at 3–5 months, Aβ plaques, impaired spatial working memory and retrieval in the Morris water maze test at around 6 months, and neurofibrillary tangles at around 12 months^{22,23}—all of these features are accelerated after ovariectomy²⁴. Four days after the ovariectomy or sham operation, mice (aged 3.5 months) received either FSH-Ab or goat IgG (200 µg per mouse, every 2 days, intraperitoneally (i.p.)) for 8 weeks. Besides displaying uterine atrophy and elevated FSH levels, ovariectomized mice showed high levels of Aβ and Tau in the hippocampus, and Aβ40 and Aβ42 in whole-brain extracts (Fig. 1a, b and Extended Data Fig. 1a, b). Brain pathology was substantially reduced in mice that were treated with FSH-Ab.

Ovariectomy also strongly induced the expression of the transcription factor C/EBPβ in hippocampal neurons (Fig. 1c and Extended Data Fig. 1c). C/EBPβ is known to activate arginine endopeptidase (AEP), a δ-secretase that cleaves amyloid precursor protein (APP) at residues

¹Department of Pathology and Laboratory Medicine, Emory University School of Medicine, Atlanta, GA, USA. ²Department of Neurology, Renmin Hospital of Wuhan University, Wuhan, China.

³Center for Translational Medicine and Pharmacology and Departments of Pharmacological Sciences and Medicine, Icahn School of Medicine at Mount Sinai, New York, NY, USA. ⁴Alamak Biosciences, Beverly, MA, USA. ⁵Department of Psychiatry and Friedman Brain Institute, Icahn School of Medicine at Mount Sinai, New York, NY, USA. ⁶Department of Anesthesiology, Emory University School of Medicine, Atlanta, GA, USA. ⁷Maine Medical Center Research Institute, Scarborough, ME, USA. ⁸Faculty of Life and Health Sciences, and Brain Cognition and Brain Disease Institute (BCBDI), Shenzhen Institute of Advanced Technology, Chinese Academy of Sciences, Shenzhen, China. ⁹These authors contributed equally: Jing Xiong, Seong Su Kang. [✉]e-mail: mone.zaidi@mssm.edu; kq.ye@siat.ac.cn

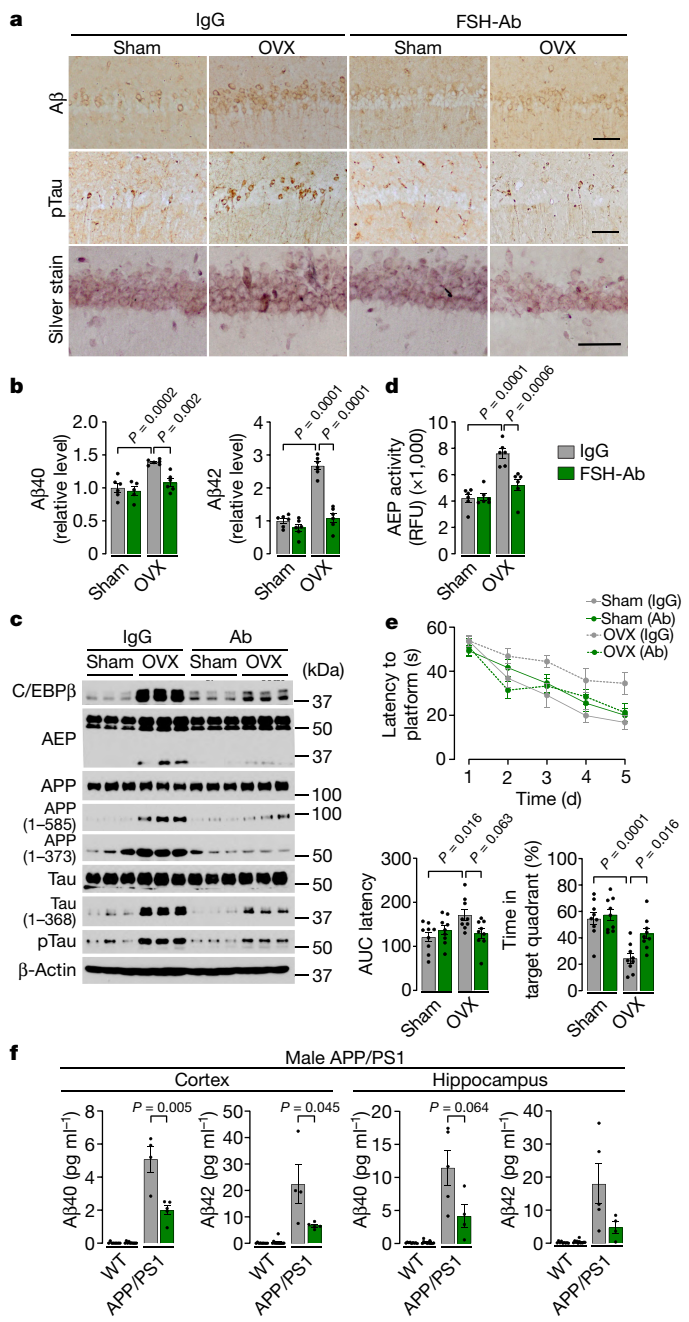


Fig. 1 | FSH-blocking antibody reverses AD neuropathology and cognitive decline in Alzheimer's mice. **a–e**, The effects of FSH-blocking antibody (FSH-Ab) or goat IgG after ovariectomy (OVX) or sham operation (Sham) of 3xTg mice (aged 3 months) on hippocampal A β , pTau and proteinaceous deposits (a); A β 40 and A β 42 (b); C/EBP β , AEP, cleaved APP, Tau and pTau (c); AEP activity (d); and parameters of spatial memory determined using Morris water maze testing (e). For a, scale bars, 50 μ m. **f**, Separate experiments show the effect of FSH-Ab or goat IgG given to male APP/PS1 mice (aged 5 months) over 4 months on hippocampal and cortical A β 40 and A β 42. Data are mean \pm s.e.m. n = 6 (b and d); n = 9 (e); and, from left to right, n = 9, n = 10, n = 4 and n = 4 (f) mice per group. Statistical analysis was performed using one-way analysis of variance (ANOVA) (b, d and e) or unpaired two-tailed Student's t-tests (f). Gel source data are provided in Supplementary Fig. 1.

Asn373 and Asn585 and Tau at Asn368 to promote A β and Tau aggregates, respectively. Deletion of AEP from 5xFAD or MAPT^{P301S} mice ameliorates amyloid plaques and neurofibrillary tangles, respectively, and rescues the memory deficits in Morris water maze testing^{25,26}. Treatment

with FSH-Ab caused an impressive reduction in ovariectomy-induced increases in expression and activation of the C/EBP β -AEP/ δ -secretase pathway, APP and Tau cleavage, and Tau phosphorylation in 3xTg mice (Fig. 1c, d and Extended Data Fig. 1b, c). FSH-Ab also reversed the ovariectomy-induced enhancement in neuronal apoptosis and reductions in dendritic spine and synapse numbers (Extended Data Fig. 1d–f). Morris water maze testing showed that ovariectomy induced a marked deficit in spatial learning and memory retrieval, evident from the increased latency of mice to mount a platform and the time spent in the platform quadrant, with no effect on motor activity (swim speed)—the altered variables were reversed in FSH-Ab-treated ovariectomized mice (Fig. 1e and Extended Data Fig. 1g).

We recognize that acute oestrogen withdrawal post-ovariectomy does not replicate the gradual menopausal transition in women, but does mirror the hormonal changes—notably reduced oestrogen and elevated FSH levels—that characterize the late menopause²⁷, when FSH levels rise considerably—again providing evidence for direct translation of our findings to this group of women. Furthermore, with no other mammal, except for certain whale species that undergo menopause, the ovariectomized mouse, albeit imperfect, has been used widely for preclinical testing of almost all menopause-related drugs²⁸.

Following our own standards for ‘contemporaneous reproduction’ of datasets in another laboratory^{6,29}, we replicated the 3xTg data at Mount Sinai using APP/PS1 mice, which have a human transgene comprising *APP^{K670N/M671L}* and *PSEN1^{ΔE9}* (ref.³⁰). The mice present with amyloid plaques at around 6 months and overt cognitive impairment at around 12 months^{30–32}. We i.p. injected male APP/PS1 mice (aged 5 months) with FSH-Ab (escalating doses from 120 to 150 μ g per mouse, 5 days per week) for 4 months. FSH-Ab prevented A β 40 and A β 42 accumulation in both the hippocampus and cortex (Fig. 1f). However, noting that APP/PS1 mice display a defect in recognition memory at around 15 months^{23,31}, as expected, we found no evidence of impaired novel-object discrimination or its alteration after treatment with FSH-Ab at 9 months (Extended Data Fig. 1h). Nonetheless, it was clear that the suppression of basal levels of serum FSH by FSH-Ab at very least prevented A β accumulation in male mice. Whether or not this translates to middle-aged female mice is unclear, but it seems to be highly probable as there is no known difference between male and female mice in serum FSH levels, in contrast to in humans³³.

Post-menopausal luteinizing hormone (LH) levels correlate with a higher incidence of AD^{15,16} and LH has been found to impair cognition through a direct action on hippocampal LH receptors (LHCGRs)^{34–36}. However, although we cannot rule out a role for high LH in AD pathogenesis on its own, we find it very unlikely that changes in LH signalling contribute to the rescue of AD pathology by FSH-Ab in ovariectomized 3xTg mice. First, our highly FSH-specific antibody does not cross-react with LH in vitro (Extended Data Fig. 1i). Second, LHCGR content in the brain of FSH-Ab-treated ovariectomized 3xTg mice is identical to that in IgG-treated mice (Extended Data Fig. 1j). Third, serum LH levels remain unchanged after treatment with FSH-Ab or FSH (Extended Data Figs. 1a and 5b). Finally, in pharmacokinetic studies, blocking FSH action using our monoclonal humanized anti-FSH β antibody (Hu6) did not alter serum LH, activin or inhibin levels³⁷.

The FSH-blocking action of FSH-Ab appears to be exerted both centrally and peripherally, in the latter case, making less free FSH available to act on brain FSH receptors (FSHRs). We found that FSH and FSH-Ab, when injected peripherally, both cross the blood–brain barrier and localize in brain tissue. AlexaFluor 750-labelled FSH, injected intravenously (i.v.), was detected in the brain by IVIS imaging, proving that FSH permeates the blood–brain barrier (Extended Data Fig. 1k). Similarly, i.p. FSH injection (5 IU) led to increased brain FSH levels (Extended Data Fig. 1l). Using four complementary methods, we

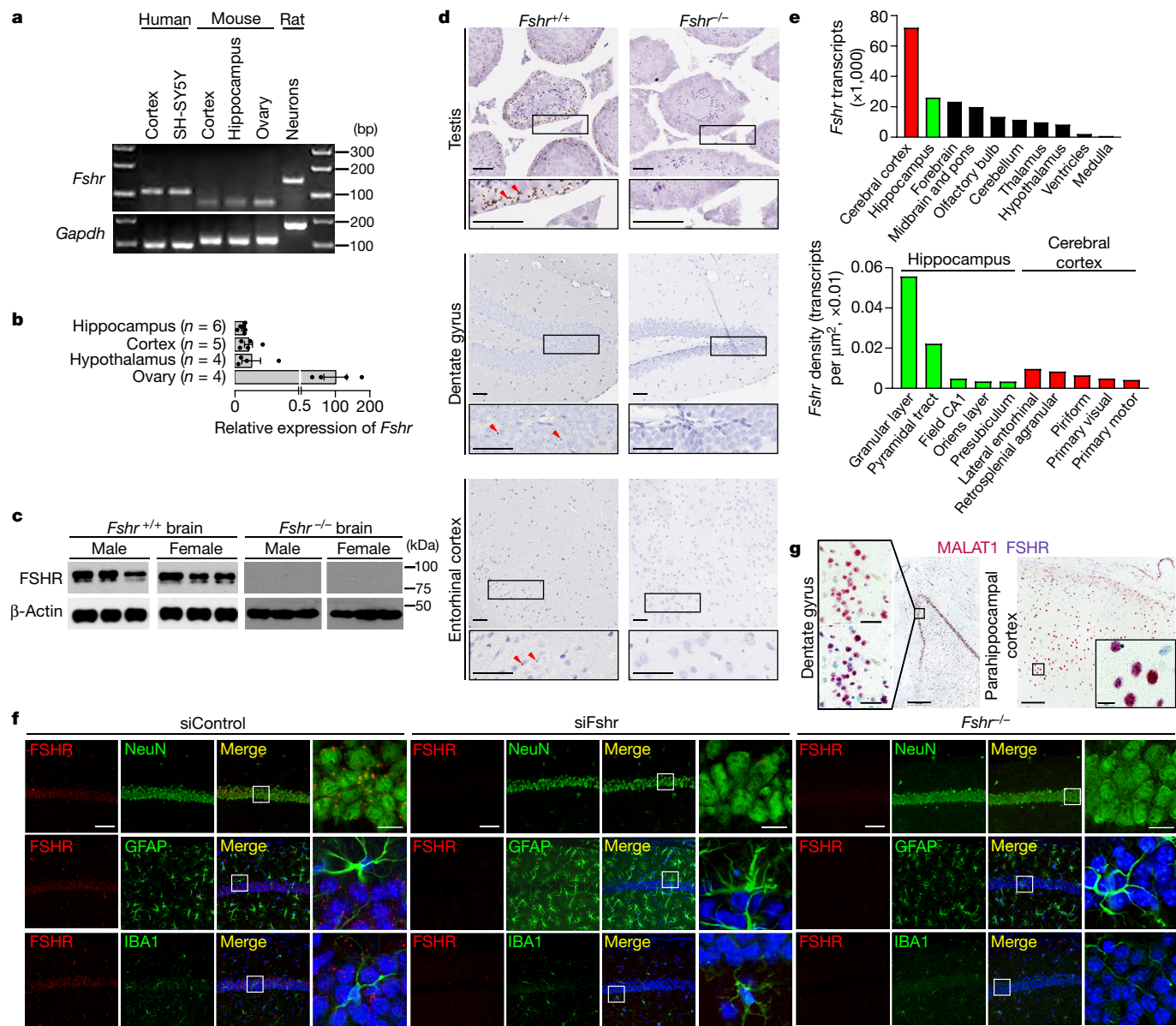


Fig. 2 | Neuronal FSH receptors in mouse and human brain. **a–c**, *Fshr* expression in human cortex, neuroblastoma cells (SH-SY5Y), mouse cortex and hippocampus, rat cortical neurons and/or mouse ovaries, determined by end-point PCR (**a**), qPCR (**b**) and/or western blotting (**c**). **d**, RNAScope signals (red arrows) in haematoxylin-stained cells from testes, and Nissl-stained neurons in the hippocampal dentate gyrus and entorhinal cortex of *Fshr*^{+/+} and *Fshr*^{-/-} mice. Scale bars, 50 μm . **e**, Transcript counts and density in multiple brain regions from 34 sections. **f**, Co-staining of FSHR, NeuN, GFAP and IBA1 in

the hippocampus after stereotactic siControl or siFshr injection in wild-type mice or in uninjected *Fshr*^{-/-} mice. Scale bars, 100 μm (main images), 10 μm (magnified images). **g**, ViewRNA signals (FSHR, dark blue; MALAT1, red) in cells from the hippocampal dentate gyrus (granular layer) (left) and parahippocampal cortex (layers V–VI) (right) from post-mortem human brain. Scale bars, 500 μm (left, main image), 50 μm (left, inset), 200 μm (right, main image), 20 μm (right, inset). For **b**, data are mean \pm s.e.m. The number of mice per group is shown.

found that peripherally injected FSH-Ab also localized to brain tissue. First, biotinylated FSH-Ab (or goat IgG) injected i.p. displayed a non-cellular localization on MAP2 co-staining (Extended Data Fig. 1m). Second, we detected ⁸⁹Zr-labelled monoclonal FSH-Ab (injected i.v.) in brain tissue using positron emission tomography (PET) imaging and γ -counting (Extended Data Fig. 1n and Supplementary Video 1). Third, using IVIS, we show that AlexaFluor750-labelled monoclonal FSH-Ab delivered i.v. localized to the brain (Extended Data Fig. 1o). Finally, specific localization in the hippocampus was confirmed by immunohistochemistry analysis of perfused brain, establishing the presence of FSH-Ab in brain tissue, external to CD31-positive cells (Extended Data Fig. 1p).

FSHR signalling in neurons

End-point and quantitative PCR (qPCR) analyses show FSHR mRNA expression in human cortex, human neuroblastoma (SH-SY5Y) cells, mouse cortex and hippocampus, and rat neurons (Fig. 2a, b). Western immunoblotting further showed an ~85 kDa FSHR protein in both male and female mouse brains, but not in brains from *Fshr*^{-/-} mice (Fig. 2c). In a separate experiment, knockdown of hippocampal *Fshr* by stereotactic injection of AAV2 expressing short interfering RNA (siRNA) targeting *Fshr* (AAV2-siFshr) led to a significant decrease in band intensity, establishing the molecular identity of the detected FSHR protein (Fig. 3a). Furthermore, RNAScope analysis of whole-brain sections revealed

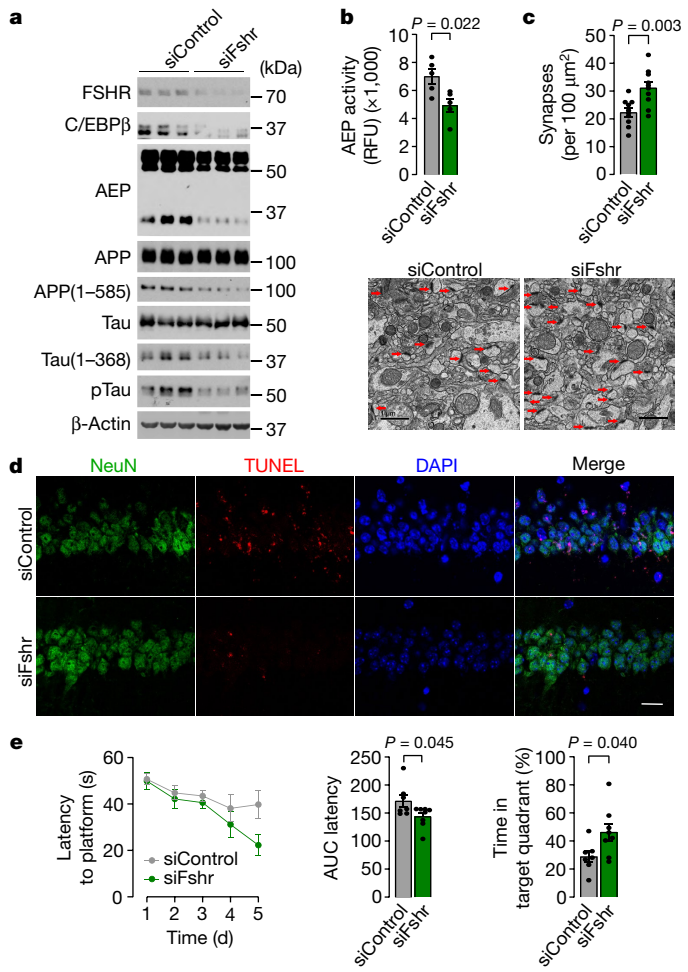


Fig. 3 | Targeted *Fshrk* knockdown in the hippocampus ameliorates AD neuropathology and impaired spatial memory. **a–e**, The effect of stereotactic injection of siFshrk versus siControl into ovariectomized 3xTg mice on total C/EBP β , AEP, cleaved APP and Tau, and FSHR levels in the whole brain (**a**); AEP activity (**b**); synapse number (transmission electron micrographs, red arrows) (**c**); cell viability (NeuN-positivity and TUNEL) (**d**); and parameters of spatial memory determined using Morris water maze testing (**e**). Scale bars, 1 μm (**c**), 20 μm (**d**). Data are mean \pm s.e.m. $n = 3$ (**a**), $n = 5 (**b**), $n = 3$ (10 sections) (**c**), and $n = 7$ or $n = 8$ (**e**) mice per group. Statistical analysis was performed using unpaired two-tailed Student's *t*-tests.$

Fshrk transcripts in cortex and hippocampus of wild-type mice, but not *Fshrk*^{-/-} mice (Fig. 2d, e). The fact that abundant *Fshrk* transcripts were present in Sertoli cells, but not Leydig cells in the same testis sections conclusively established probe specificity (Fig. 2d). *Fshrk* expression was also detected in other brain regions and subregions, with the highest *Fshrk* density noted in the granular cell layer of the dentate gyrus, where transcripts localized primarily to Nissl-stained neurons (Fig. 2d, e). Using immunofluorescence analysis, FSHRs were found to co-localize with NeuN in hippocampal neurons, with little-to-no expression in glial cells (Fig. 2f). Importantly, FSHR immunostaining was abrogated after stereotactic hippocampal injection of AAV2-siFshrk, and was absent in similarly stained sections from *Fshrk*^{-/-} mouse brains (Fig. 2f). Consistent with the mouse brain, a ViewRNA analysis showed that *FSHR* transcripts co-localized with the non-coding RNA *MALAT1* in the granular cell layer of the hippocampal dentate gyrus and in the parahippocampal cortex (Fig. 2g).

We studied a role for the C/EBP β –AEP/ δ -secretase pathway in mediating FSH action using human neuroblastoma SH-SY5Y cells and primary rat cortical neurons. Treatment with FSH (30 ng ml⁻¹) increased C/EBP β

and activated AEP in a time-dependent manner in both cell types, and the activated AEP cleaved both APP and Tau (Extended Data Fig. 2a). qPCR showed a time-dependent increase in *CEBPB*, *LGMN*, *APP* and *MAPT* expression, as well as enhanced AEP activity after FSH treatment (Extended Data Fig. 2b, c). Consistent with the known proinflammatory responses to C/EBP β activation³⁸, FSH also induced the expression of the pro-inflammatory cytokines IL-1 β and IL-6 (Extended Data Fig. 2d). Notably, the FSH-induced increases in C/EBP β expression, AEP activity, and APP and Tau cleavage were decreased in the two cell types after infection with human siFSHR and rat AAV2-siFshrk, respectively (Extended Data Fig. 2e). Similarly, in SH-SY5Y cells, siFshrk attenuated FSH-induced increases in *CEBPB*, *LGMN*, *APP* and *MAPT* mRNA, AEP activity, and secreted IL-1 β and IL-6 (Extended Data Fig. 2f–h). We also infected both cell types with a lentivirus (LV) containing short hairpin RNA against *Cebpb* (shCebpb) and AAV-AEP C189S , an AAV-expressing inactive AEP. Knocking down C/EBP β or inactivating AEP substantially reduced the FSH-induced cleavage of APP and Tau (Extended Data Fig. 3a). Co-staining of cortical neurons confirmed that the FSH-induced increases in A β , phosphorylated Tau (pTau), cleaved APP and Tau, and AEP activity were reduced in cells infected with both viruses (Extended Data Fig. 3b, c). Collectively, these data confirm that FSH acts on FSHR to activate the C/EBP β –AEP/ δ -secretase pathway.

To examine the signalling mechanisms, we studied the effect of FSH on ERK1/2, SRPK2 and AKT in both cell types. Notably, MAPK-induced phosphorylation of residue Thr188 of C/EBP β regulates its transcriptional activity³⁹. Similarly, AKT phosphorylates SRPK2, which in turn activates AEP by phosphorylating residue Ser226 (ref. ⁴⁰). We found that total C/EBP β and pC/EBP β and active AEP progressively increased from 5 min after FSH exposure, whereas ERK1/2, AKT and SFRP2 phosphorylation peaked at ~30 min, with a delayed rise in NF- κ B p65 (Extended Data Fig. 3d). Pertussis toxin, which decouples FSHRs from G α_i protein^{6,41}, inhibited FSH-induced C/EBP β and AEP activation and AKT phosphorylation (Extended Data Fig. 3e). Consistent with maximal inhibition of the G α_i pathway, the adenylate cyclase inhibitor SQ22536 had no effect, whereas the AKT inhibitor AKT1-2 attenuated FSH-induced C/EBP β expression, AEP cleavage and SRPK2 phosphorylation, without an effect on ERK1/2 (Extended Data Fig. 3e). Similarly, whereas the MEK1 inhibitor PD98059 blocked FSH-induced C/EBP β , AEP and SRPK2 activation, AKT was unaffected (Extended Data Fig. 3e). Together, these data suggest that, in both human and rat neurons, FSH phosphorylates AKT, ERK1/2 and SRPK2 leading to the activation of C/EBP β –AEP/ δ -secretase and subsequent proteolytic cleavage of APP and Tau.

Neuronal *Fshrk* knockdown decreases AD pathology

We examined whether the selective ablation of the *Fshrk* in the hippocampus mimics the effect of systemic FSH-Ab. In brief, 3xTg mice underwent ovariectomy 7 days after stereotactic injection of AAV2-siFshrk or scrambled control viral suspension (2 μl at 0.25 $\mu\text{l min}^{-1}$, 2 \times 10⁹ vector genomes per μl) into the hippocampus. AAV2-siFshrk-injected mice showed substantial decreases in FSHR protein and mRNA; total C/EBP β and AEP; cleaved APP; cleaved and phosphorylated Tau; A β and its isoforms A β 40 and A β 42; and AEP activity (Fig. 3a, b and Extended Data Fig. 4a–c). The inhibition was recapitulated at the mRNA level for *Cebpb*, *Lgmn*, *App* and *Mapt* (Extended Data Fig. 4a). Similarly, compared with control-siRNA-injected mice, AAV2-siFshrk-injected mice showed increases in dendritic spines and synapse number, and dampened neuronal apoptosis (Fig. 3c, d and Extended Data Fig. 4d). Testing using the Morris water maze revealed significant enhancements in spatial memory, notably, reduced latency to mount a platform and increased time spent in the platform quadrant in AAV2-siFshrk-injected mice (Fig. 3e). Together, these data provide clear evidence for a role of hippocampus-resident, mainly neuronal, FSHRs in mediating, at least in part, the effects of FSH on AD pathogenesis. However, despite the preferential infection of neurons by AAV2 (serotype 2), we cannot

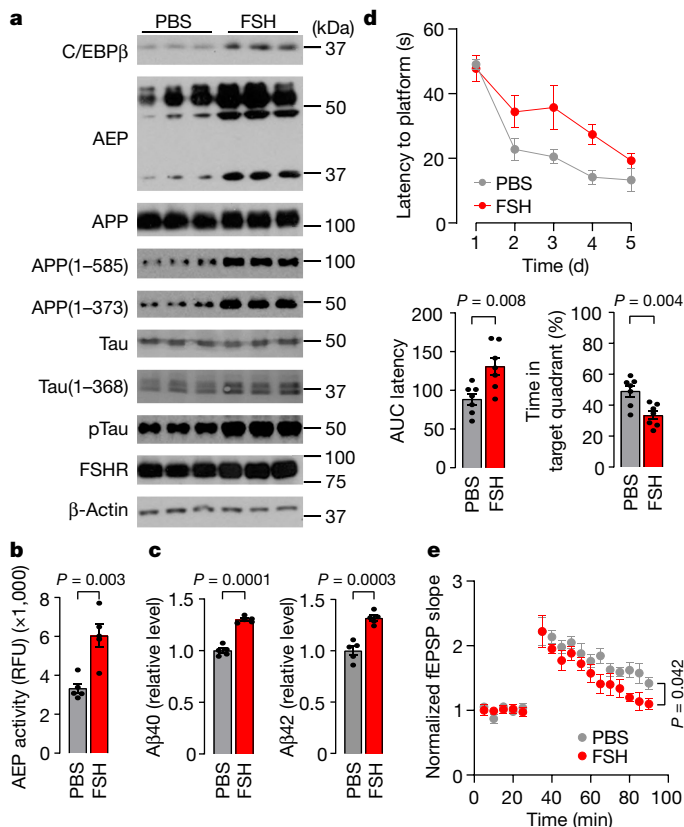


Fig. 4 | Recombinant FSH induces AD pathologies and cognitive decline in 3xTg Mice. **a–d**, The effect of injecting female 3xTg mice with recombinant human FSH on whole-brain C/EBP β , AEP, cleaved APP and Tau proteins (a); AEP activity (b); A β 40 and A β 42 (c); and parameters of spatial memory determined using Morris water maze testing (d). **e**, The effect of FSH on long-term potentiation (LTP) shown as fEPSPs before (grey) and 60 min after (red) theta-burst stimulation. Data are mean \pm s.e.m. $n = 5$ (b and c), $n = 7$ (d) and $n = 4$ (e) mice per group. Statistical analysis was performed using unpaired two-tailed Student's *t*-tests.

exclude the possibility that non-neuronal glial cells are also infected by AAV siRNA^{42,43}. However, the fact that we almost exclusively find FSHRs on NeuN-positive neurons and not in glial cells (Fig. 2f) establishes that the effects of *Fsh* knockdown on the AD phenotype are mediated largely through neurons.

Systemic FSH triggers AD pathology

The i.p. injection of female 3xTg mice (aged 2.5 months) with a single dose of 2 IU, 5 IU or 10 IU of recombinant human FSH showed a dose-dependent increase in serum human FSH levels at 24 h (Extended Data Fig. 5a). However, as expected, endogenous mouse FSH levels remained stable at around 10 mIU ml $^{-1}$, and serum LH levels did not change (Extended Data Fig. 5a, b). The elevation in serum FSH at 5 IU was similar to that observed post-ovariectomy (compare with Extended Data Fig. 1a), as well as during the human menopausal transition¹⁷. Notably, we also detected an increase in FSH in brain lysates after i.p. injection, suggesting that FSH crosses the blood–brain barrier (Extended Data Fig. 1l). FSH (5 IU per mouse, i.p.) injected daily for 3 months caused a marked increase in brain C/EBP β and AEP, and a robust activation of AEP to cleave APP and Tau (Fig. 4a, b and Extended Data Fig. 5h, i). Similarly, FSH induced pTau, A β 40 and A β 42 isoforms, and plaque formation was confirmed in hippocampal sections by thioflavin-S staining, and in the cortex and the cornu ammonis 1 (CA1) and dentate gyrus regions of the hippocampus by silver staining (Fig. 4c and Extended

Data Fig. 5c, d, j). Importantly, FSH-induced enhancements in C/EBP β and AEP occurred in A β - and pTau-bearing NeuN-positive neurons (Extended Data Fig. 5l). This, together with the selective expression of FSHR in human and mouse neurons (Fig. 2), further confirm a primary neuronal action of FSH. Furthermore, FSH triggered *Cebpb*, *Lgmn*, *App* and *Mapt* expression (Extended Data Fig. 5e), and caused marked apoptosis in hippocampal and cortical neurons, with reduced dendritic spine and synapse numbers (Extended Data Fig. 5f, g, k). Testing using the Morris water maze showed that FSH-injected mice had impaired spatial memory associated with reduced long-term potentiation (field excitatory post-synaptic potentials (fEPSPs)) in the CA1 hippocampal region (Fig. 4d, e). Taken together, systemic FSH over 3 months caused a marked acceleration of AD pathology in female 3xTg mice.

To mimic the mid- and late-menopausal transition, during which FSH levels rise in the face of unaltered serum oestrogen⁴⁴, we replaced oestrogen in ovariectomized 3xTg mice. Serum oestrogen was clamped close to basal levels (~75 pg ml $^{-1}$) by s.c. implanting 17 β -estradiol 90-day-release pellets (0.36 mg) before i.p. FSH injections (5 IU daily) given for 3 months (Extended Data Fig. 6a). Even in this oestrogen-replete state, FSH induced C/EBP β and AEP expression, AEP activation, A β and pTau accumulation, APP and Tau cleavage, and Tau phosphorylation (compare Extended Data Fig. 6b–d with Fig. 4a, b and Extended Data Fig. 5c, d). These data provide unequivocal evidence that the effect of FSH is independent of oestrogen in female mice. Moreover, i.p. FSH injections (5 IU per mouse) for 3 months triggered identical neuropathology and cognitive impairment in male 3xTg mice (compare Extended Data Fig. 7 with Fig. 4 and Extended Data Fig. 5). Thus, while FSH triggers overt AD-like features in both female and male 3xTg mice, the phenotype is exacerbated after ovariectomy (high FSH) in female mice and, by implication, after the menopause in women.

As mouse A β barely oligomerizes to form plaques, aging wild-type mice do not display human-like AD features, despite increases in mouse A β production⁴⁵. To provide a non-transgenic control for 3xTg mice (Fig. 4), we studied the effect of high FSH in wild-type mice aged 3 months. Although i.p. treatment of FSH (5 IU per day for 3 months) increased C/EBP β and AEP expression, AEP activity and the cleavage of mouse APP and Tau, it did not yield A β plaques or trigger memory impairment (Extended Data Fig. 8a–e). Thus, mice must express human APP to form A β plaques and induce cognitive decline in response to FSH. However, both 3xTg and APP/PS1 mice overexpress human A β transgenically at levels that are potentially neurotoxic. By contrast, in APP-KI mice, three amino acid substitutions (G601R, F606Y and R609H) are knocked into exon 14 of the A β -encoding *App* gene resulting in the expression of oligomerizable human A β at basal levels. FSH (5 IU per day for 3 months, i.p.) injected into female APP-KI mice (aged around 3 months) increased C/EBP β and AEP expression and APP cleavage, and induced A β plaques in the hippocampus and/or cortex, A β 40 and A β 42 accumulation in the whole brain, and apoptosis in the hippocampus (Extended Data Fig. 8f–h, i, k). Although Tau is not mutated in APP-KI mice, there was an increase in the cleavage of endogenous Tau (Extended Data Fig. 8f). Morris water maze testing of FSH-treated APP-KI mice revealed impaired spatial memory (Extended Data Fig. 8j). Collectively, the responsiveness of APP-KI mice to FSH further reaffirms a role for FSH as a driver of AD in a model that closely resembles the human disease. It also rules out confounding effects of toxic levels of transgenic A β overexpression in 3xTg and APP/PS1 mice.

FSH induces AD pathology through C/EPB β

We generated compound *Cebpb*^{+/−} 3xTg mutant mice on a C57BL/6 background by crossing 3xTg with *Cebpb*^{+/−} mice. We i.p. injected 2.5- to 3-month-old compound mutant mice with FSH (5 IU per mouse) daily for 3 months. *Cebpb*^{−/−} mice were not used due to a potentially confounding metabolic phenotype⁴⁶. Haploinsufficiency of *Cebpb* led to attenuated baseline events—notably, lower AEP activation and APP

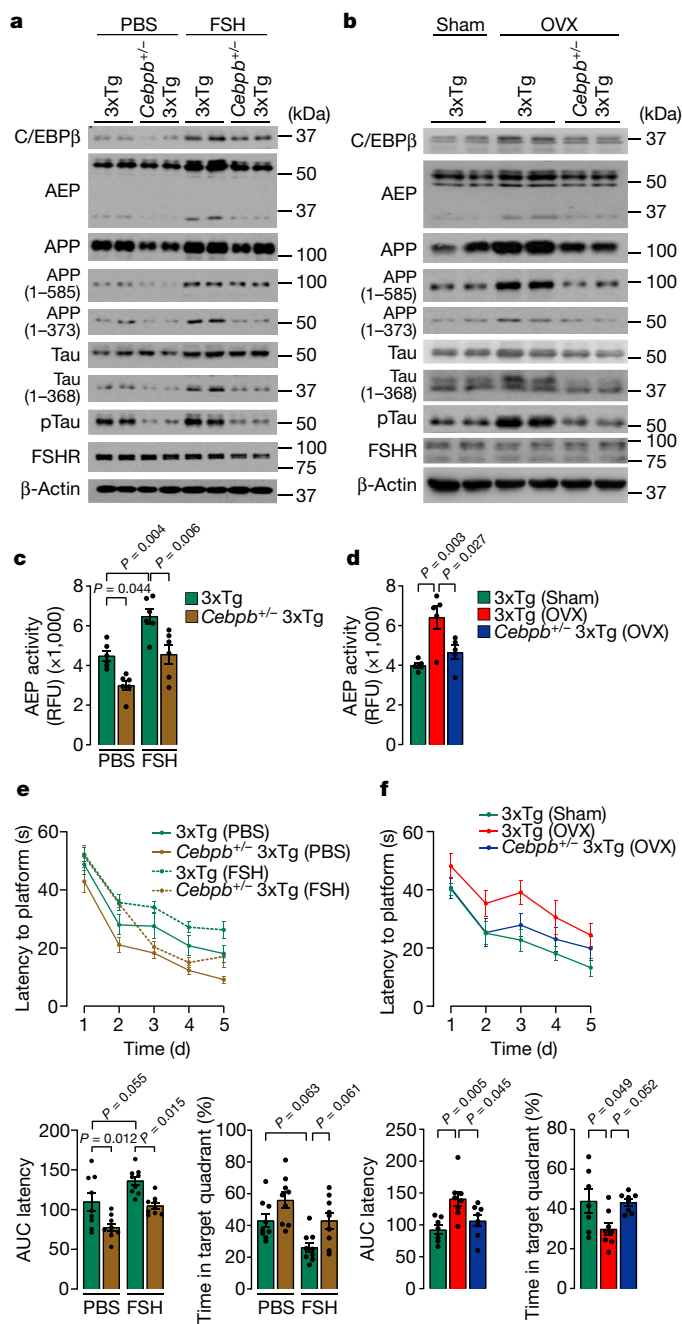


Fig. 5 | FSH-induced AD pathology is dampedened in *Cebpb*^{+/−} 3xTg mice. **a–f**, The effect of injecting recombinant human FSH (**a**, **c** and **e**) or ovariectomy (**b**, **d**, **f**) in 3xTg mice or compound mutant *Cebpb*^{+/−} 3xTg mice on C/EBPβ, AEP, cleaved APP, cleaved Tau, pTau and FSHR (**a**, **b**); AEP activity (**c**, **d**); and parameters of spatial memory determined using Morris water maze testing (**e**, **f**). Data are mean \pm s.e.m. $n = 6$ (**c**), $n = 5$ (**d**), $n = 9$ (**e**), and $n = 7$ or $n = 8$ (**f**) mice per group. Statistical analysis was performed using one-way ANOVA.

and Tau cleavage (Fig. 5a, c). In 3xTg mice, FSH induced AEP activity, APP and Tau cleavage, and A β and pTau accumulation, whereas the responses to FSH were attenuated in *Cebpb*^{+/−} 3xTg mice (Fig. 5a and Extended Data Fig. 9b–d). FSH-induced increases in *Cebpb*, *Lgmn*, *App* and *Mapt* expression were similarly attenuated in *Cebpb*^{+/−} 3xTg mice (Extended Data Fig. 9a). C/EBPβ haploinsufficiency also reversed the decreases in dendritic spine numbers, as well as the cognitive deficit induced by FSH (Fig. 5e and Extended Data Fig. 9e, f). As FSH is elevated after ovariectomy (Extended Data Fig. 1a), we predicted that the effects of ovariectomy in inducing AD pathology and cognitive decline

would also be attenuated in compound *Cebpb*^{+/−} 3xTg mice. Indeed, FSH-induced *Cebpb*, *Lgmn*, *App* and *Mapt* expression, AEP activation, APP and Tau cleavage, A β and pTau accumulation, dendritic spine deficits and cognition defects were all lower in *Cebpb*^{+/−} 3xTg mice compared with 3xTg mice (Fig. 5b, d, f and Extended Data Fig. 10a–f). Taken together, these data provide strong genetic evidence for a primary role for C/EBPβ in mediating the AD pathology induced by FSH.

Discussion

The idea that the brain is a target for FSH is consistent with research that has established broad ubiquity for pituitary hormone action—a stark departure from the long-held view that pituitary glycoproteins act solely on endocrine targets⁴⁷. We first discovered an extragonadal action of FSH by demonstrating high bone mass in FSH β haploinsufficient mice that were eugonadal⁴¹. Studies have since documented the existence of functional FSHRs on bone cells, adipocytes and hepatocytes, and have established that selective FSH blockade—such as by FSH-Ab used here—stimulates new bone synthesis, reduces body fat, increases thermogenesis and lowers serum cholesterol^{5–7}. In gonadal cells, FSH is also known to activate C/EBPβ^{48,49}, which has been associated with AD pathology, particularly as it transactivates pro-inflammatory genes that mediate the chronic inflammation of AD³⁸. We previously showed that the spatiotemporal dysregulation of the C/EBPβ–AEP/δ-secretase pathway mediates AD pathology⁵⁰.

Thus, our observations that link FSH and AD through the C/EBPβ–AEP/δ-secretase pathway, taken together with the strong clinical association of AD with rising serum FSH levels, provide the basis for an array of actionable targets for AD in post-menopausal women. Furthermore, as FSH levels also rise in aging men³³, our finding that systemic FSH induces and FSH-Ab rescues AD pathology in both sexes provides an opportune window for testing an anti-FSH agent in humans. Given that blocking FSH not only reduces bone loss, body fat and serum cholesterol^{3,5,6,21}, but also dampens AD pathology in mice as shown here, an agent, such as a highly targeted anti-FSH antibody³⁷, could be tested in the future for the co-therapy of osteoporosis, obesity, dyslipidaemia and Alzheimer’s disease.

Online content

Any methods, additional references, Nature Research reporting summaries, source data, extended data, supplementary information, acknowledgements, peer review information; details of author contributions and competing interests; and statements of data and code availability are available at <https://doi.org/10.1038/s41586-022-04463-0>.

1. Sowers, M. et al. Changes in body composition in women over six years at midlife: ovarian and chronological aging. *J. Clin. Endocrinol. Metab.* **92**, 895–901 (2007).
2. Sowers, M. R. et al. Hormone predictors of bone mineral density changes during the menopausal transition. *J. Clin. Endocrinol. Metab.* **91**, 1261–1267 (2006).
3. Guo, Y. et al. Blocking FSH inhibits hepatic cholesterol biosynthesis and reduces serum cholesterol. *Cell Res.* **29**, 151–166 (2019).
4. Han, X. et al. A novel follicle-stimulating hormone vaccine for controlling fat accumulation. *Theriogenology* **148**, 103–111 (2020).
5. Ji, Y. et al. Epitope-specific monoclonal antibodies to FSH β increase bone mass. *Proc. Natl. Acad. Sci. USA* **115**, 2192–2197 (2018).
6. Liu, P. et al. Blocking FSH induces thermogenic adipose tissue and reduces body fat. *Nature* **546**, 107–112 (2017).
7. Geng, W. et al. Immunization with FSH β fusion protein antigen prevents bone loss in a rat ovariectomy-induced osteoporosis model. *Biochem. Biophys. Res. Commun.* **434**, 280–286 (2013).
8. Fisher, D. W., Bennett, D. A. & Dong, H. Sexual dimorphism in predisposition to Alzheimer’s disease. *Neurobiol. Aging* **70**, 308–324 (2018).
9. Andersen, K. et al. Gender differences in the incidence of AD and vascular dementia: the EURODEM studies. *EURODEM Incidence Research Group. Neurology* **53**, 1992–1997 (1999).
10. Marongiu, R. Accelerated ovarian failure as a unique model to study peri-menopause influence on Alzheimer’s disease. *Front. Aging Neurosci.* **11**, 242 (2019).
11. Matyi, J. M., Rattinger, G. B., Schwartz, S., Buhusi, M. & Tschanz, J. T. Lifetime estrogen exposure and cognition in late life: the Cache County study. *Menopause* **26**, 1366–1374 (2019).

12. Zandi, P. P. et al. Hormone replacement therapy and incidence of Alzheimer disease in older women: the Cache County Study. *JAMA* **288**, 2123–2129 (2002).
13. O'Brien, J., Jackson, J. W., Grodstein, F., Blacker, D. & Weuve, J. Postmenopausal hormone therapy is not associated with risk of all-cause dementia and Alzheimer's disease. *Epidemiol. Rev.* **36**, 83–103 (2014).
14. Shumaker, S. A. et al. Conjugated equine estrogens and incidence of probable dementia and mild cognitive impairment in postmenopausal women: Women's Health Initiative Memory Study. *JAMA* **291**, 2947–2958 (2004).
15. Short, R. A., Bowen, R. L., O'Brien, P. C. & Graff-Radford, N. R. Elevated gonadotropin levels in patients with Alzheimer disease. *Mayo Clin. Proc.* **76**, 906–909 (2001).
16. Bowen, R. L., Isley, J. P. & Atkinson, R. L. An association of elevated serum gonadotropin concentrations and Alzheimer disease? *J. Neuroendocrinol.* **12**, 351–354 (2000).
17. Randolph, J. F. Jr et al. Change in follicle-stimulating hormone and estradiol across the menopausal transition: effect of age at the final menstrual period. *J. Clin. Endocrinol. Metab.* **96**, 746–754 (2011).
18. Epperson, C. N., Sammel, M. D. & Freeman, E. W. Menopause effects on verbal memory: findings from a longitudinal community cohort. *J. Clin. Endocrinol. Metab.* **98**, 3829–3838 (2013).
19. Greendale, G. A. et al. Effects of the menopause transition and hormone use on cognitive performance in midlife women. *Neurology* **72**, 1850–1857 (2009).
20. Meyer, P. M. et al. A population-based longitudinal study of cognitive functioning in the menopausal transition. *Neurology* **61**, 801–806 (2003).
21. Zhu, L. L. et al. Blocking antibody to the β-subunit of FSH prevents bone loss by inhibiting bone resorption and stimulating bone synthesis. *Proc. Natl Acad. Sci. USA* **109**, 14574–14579 (2012).
22. Oddo, S. et al. Triple-transgenic model of Alzheimer's disease with plaques and tangles: intracellular Aβ and synaptic dysfunction. *Neuron* **39**, 409–421 (2003).
23. Webster, S. J., Bachstetter, A. D., Nelson, P. T., Schmitt, F. A. & Van Eldik, L. J. Using mice to model Alzheimer's dementia: an overview of the clinical disease and the preclinical behavioral changes in 10 mouse models. *Front. Genet.* **5**, 88 (2014).
24. Carroll, J. C. et al. Progesterone and estrogen regulate Alzheimer-like neuropathology in female 3xTg-AD mice. *J. Neurosci.* **27**, 13357–13365 (2007).
25. Zhang, Z. et al. Cleavage of tau by asparagine endopeptidase mediates the neurofibrillary pathology in Alzheimer's disease. *Nat. Med.* **20**, 1254–1262 (2014).
26. Zhang, Z. et al. Delta-secretase cleaves amyloid precursor protein and regulates the pathogenesis in Alzheimer's disease. *Nat. Commun.* **6**, 8762 (2015).
27. Rocca, W. A. et al. Increased risk of cognitive impairment or dementia in women who underwent oophorectomy before menopause. *Neurology* **69**, 1074–1083 (2007).
28. Tokuyama, N. et al. Individual and combining effects of anti-RANKL monoclonal antibody and teriparatide in ovariectomized mice. *Bone Rep.* **2**, 1–7 (2015).
29. Rosen, C. J. & Zaidi, M. Contemporaneous reproduction of preclinical science: a case study of FSH and fat. *Ann. N. Y. Acad. Sci.* **1404**, 17–19 (2017).
30. Minkeviciene, R. et al. Age-related decrease in stimulated glutamate release and vesicular glutamate transporters in APP/PS1 transgenic and wild-type mice. *J. Neurochem.* **105**, 584–594 (2008).
31. Onos, K. D. et al. Enhancing face validity of mouse models of Alzheimer's disease with natural genetic variation. *PLoS Genet.* **15**, e1008155 (2019).
32. Volianskis, A., Kostner, R., Molgaard, M., Hass, S. & Jensen, M. S. Episodic memory deficits are not related to altered glutamatergic synaptic transmission and plasticity in the CA1 hippocampus of the APPswe/PS1deltaE9-deleted transgenic mice model of ss-amyloidosis. *Neurobiol. Aging* **31**, 1173–1187 (2010).
33. Araujo, A. B. & Wittert, G. A. Endocrinology of the aging male. *Best Pract. Res. Clin. Endocrinol.* **25**, 303–319 (2011).
34. Casadesus, G. et al. Increases in luteinizing hormone are associated with declines in cognitive performance. *Mol. Cell. Endocrinol.* **269**, 107–111 (2007).
35. Berry, A., Tomidokoro, Y., Ghiso, J. & Thornton, J. Human chorionic gonadotropin (a luteinizing hormone homologue) decreases spatial memory and increases brain amyloid-β levels in female rats. *Horm. Behav.* **54**, 143–152 (2008).
36. Liu, T., Wimalasena, J., Bowen, R. L. & Atwood, C. S. Luteinizing hormone receptor mediates neuronal pregnenolone production via up-regulation of steroidogenic acute regulatory protein expression. *J. Neurochem.* **100**, 1329–1339 (2007).
37. Gera, S. et al. First-in-class humanized FSH blocking antibody targets bone and fat. *Proc. Natl Acad. Sci. USA* **117**, 28971–28979 (2020).
38. Straccia, M. et al. Pro-inflammatory gene expression and neurotoxic effects of activated microglia are attenuated by absence of CCAAT/enhancer binding protein β. *J. Neuroinflammation* **8**, 156 (2011).
39. Ramji, D. P. & Foka, P. CCAAT/enhancer-binding proteins: structure, function and regulation. *Biochem. J.* **365**, 561–575 (2002).
40. Wang, Z. H. et al. Delta-secretase phosphorylation by SRPK2 enhances its enzymatic activity, provoking pathogenesis in Alzheimer's disease. *Mol. Cell* **67**, 812–825 (2017).
41. Sun, L. et al. FSH directly regulates bone mass. *Cell* **125**, 247–260 (2006).
42. Hammond, S. L., Leek, A. N., Richman, E. H. & Tjalkens, R. B. Cellular selectivity of AAV serotypes for gene delivery in neurons and astrocytes by neonatal intracerebroventricular injection. *PLoS ONE* **12**, e0188830 (2017).
43. von Jonquieres, G. et al. Recombinant human myelin-associated glycoprotein promoter drives selective AAV-mediated transgene expression in oligodendrocytes. *Front. Mol. Neurosci.* **9**, 13 (2016).
44. Randolph, J. F. Jr. et al. Reproductive hormones in the early menopausal transition: relationship to ethnicity, body size, and menopausal status. *J. Clin. Endocrinol. Metab.* **88**, 1516–1522 (2003).
45. Ashe, K. H. & Zahs, K. R. Probing the biology of Alzheimer's disease in mice. *Neuron* **66**, 631–645 (2010).
46. Millward, C. A. et al. Mice with a deletion in the gene for CCAAT/enhancer-binding protein β are protected against diet-induced obesity. *Diabetes* **56**, 161–167 (2007).
47. Zaidi, M. et al. Actions of pituitary hormones beyond traditional targets. *J. Endocrinol.* **237**, R83–R98 (2018).
48. Silverman, E., Eimerl, S. & Orly, J. CCAAT enhancer-binding protein β and GATA-4 binding regions within the promoter of the steroidogenic acute regulatory protein (StAR) gene are required for transcription in rat ovarian cells. *J. Biol. Chem.* **274**, 17987–17996 (1999).
49. Sirois, J. & Richards, J. S. Transcriptional regulation of the rat prostaglandin endoperoxide synthase 2 gene in granulosa cells. Evidence for the role of a cis-acting C/EBPβ promoter element. *J. Biol. Chem.* **268**, 21931–21938 (1993).
50. Wang, H., Liu, X., Chen, S. & Ye, K. Spatiotemporal activation of the C/EBPβ/δ-secretase axis regulates the pathogenesis of Alzheimer's disease. *Proc. Natl Acad. Sci. USA* **115**, E12427–E12434 (2018).

Publisher's note Springer Nature remains neutral with regard to jurisdictional claims in published maps and institutional affiliations.

© The Author(s), under exclusive licence to Springer Nature Limited 2022

Methods

Transgenic mice

3xTg mice were obtained from Jackson Laboratory (034830). The mice have a transgene with mutated human *APP*^{K670N/M671L} and *MAPT*^{P301L}, and a knockin mutation *Psen1*^{M146V} and display AD neuropathology and a decline in long-term memory at around 3 to 4 months²². Mutant *Cebpb* mice⁵¹ were maintained at the Emory University School of Medicine as heterozygotes on C57BL/6 and 129Sv backgrounds. The two strains were crossed to generate viable F₁ hybrid wild-type and *Cebpb*^{+/−} littermates; the latter were then crossed with 3xTg mice to generate compound *Cebpb*^{+/−} 3xTg and *Cebpb*^{+/−} 3xTg mutants. *APP/PS1* mice, which were obtained from Jackson Laboratory (034829) and bred at the Icahn School of Medicine at Mount Sinai (ISMMS), have a human transgene comprising *APP*^{K670N/M671L} and *PSEN1*^{AE9} (ref.³⁰). *APP/PS1* mice develop amyloid plaques at 6 months and overt cognitive impairment at a later age of 15 months; they do not display neurofibrillary tangles^{30–32}. These mice, when bred on a pure C57BL/6J background, show evidence of sudden death (27%) due to seizure activity (65%)⁵². Our losses were mostly in the 5 month, drug-naïve period (13 deaths out of 28), followed by 5 deaths during the 4 month treatment with IgG (3 deaths) or FSH-Ab (2 deaths). *APP/PS1* mice were genotyped and regenotyped for human *PSEN1*, followed by qPCR for human *APP*. In contrast to 3xTg and *APP/PS1* transgenic mice, in *APP-KI* mice, three amino acid substitutions (G601R, F606Y and R609H) are knocked into Aβ-coding exon 14 of the *App* gene—this results in the non-transgenic expression at basal levels of readily oligomerizable human Aβ (Jackson Laboratory, 030898). For studies using 3xTg and *APP-KI* mice, sample sizes were determined on the basis of previous studies by K.Y. and other groups. Mice were randomly selected to be assigned into separate groups—namely, ovariectomy or sham-operation, PBS or FSH, IgG or FSH-Ab, and siControl or siFsh. Key behavioural studies at Emory University were conducted in the Rodent Behavioral Core by technicians who were unaware of the mouse groups. Animal care and handling were performed according to NIH animal care guidelines at both the Emory University School of Medicine and the ISMMS. The protocols were reviewed and approved by the respective Institutional Animal Care and Use Committees.

Ovariectomy

Each mouse underwent shaving and prepping of the lower back using 70% ethanol and sterile PBS, followed by washing with povidone iodine solution before the surgery. A ~0.5 cm skin incision and a further incision through the muscle layer allowed access to the peritoneal cavity. The ovaries were visualized through the muscle layer and, one at a time, extracted through the incision, tied off and removed. The muscle layer was then sutured followed by closure of the external incision with wound clips. Each mouse was placed in a clean cage and allowed to recover from the anaesthesia, and returned to home cage after observation of normal behaviour and ambulation.

Stereotactic injection

AAV2-siFsh virus (iAAV04355302) and control virus (iAAV01502) from Applied Biological Materials were injected stereotactically into female 3xTg mice (aged 3 months) under isoflurane anaesthesia. We used the following coordinates for bilateral intracerebral injections: −2.1 mm anteroposterior and −1.8 mm mediolateral from the bregma, and −1.5 mm dorsoventral from the dural surface. Viral suspension (2 µl) containing 2×10^9 vector genomes per µl was placed into each site at a rate of 0.25 µl min^{−1} using a 10 µl glass syringe with a fixed needle. The needle remained in place for 5 min and was removed slowly over 2 min. Mice were placed on a heating pad until they turned from a supine to a prone position, indicative of recovery from anaesthesia. The mice underwent ovariectomy 7 days after stereotactic injection.

Antibodies and reagents

Please refer to the Reporting Summary and Supplementary Table 1 for details, including prior validation of each antibody. Antibodies against C/EBPβ (H-7, sc-7962, H-7, 1:1,000 dilution for western blotting and 1:200 for immunofluorescence), C/EBPβ (rabbit polyclonal, sc-150, 1:1,000 dilution) and FSHβ (sc-374452, C12, 1:1,000 dilution for western blotting) were from Santa Cruz; antibodies against AEP (6E3) were a gift from C. Watts (1:1,000 dilution for western blotting); antibodies against FSHR (PA5-50963, 1:1,000 dilution for western blotting and 1:200 for immunofluorescence), pTau(Ser202-Thr205) (MN1020, AT8, 1:1,000 dilution for western blotting and 1:200 for immunofluorescence and immunohistochemistry) and IBA1 (PA5-18039, 1:500 dilution for immunofluorescence) were from Thermo Fisher Scientific; antibodies against Legumain (LGMD, D6S4H) (93627, 1:2,000 dilution for western blotting and 1:500 for immunofluorescence), AKT (4691s, 1:1,000 dilution for western blotting), pAKT^{S473} (rabbit polyclonal, 9271s, 1:1,000 dilution for western blotting), ERK1/2 (9102s, 1:1,000 dilution for western blotting), pERK1/2 (9106s, 1:2,000 dilution for western blotting) were purchased from Cell Signaling Technology; antibodies against NeuN (MAB377, 1:300 dilution for immunofluorescence), NeuN (ABN90, 1:600 dilution for immunofluorescence), Tau(210–241)(Tau-5, MAB361, 1:2,000 dilution for western blotting), β-actin (A5316, 1:3,000 dilution for western blotting) and GFAP (MAB360, GA5, 1:400 dilution for immunofluorescence) were from Sigma-Aldrich; antibodies against Aβ (800701, 4G8, 1:400 dilution for immunohistochemistry and immunofluorescence) were obtained from BioLegend; and antibodies against SRPK2 (611118, 23/SRPK2, 1:2,000 for western blotting) were from BD Biosciences. Antibodies against pAEP^{S226}, Tau(1–368), APP(1–585), APP(1–373) and pSRPK2(T492) were developed in the K.Y.'s lab (1:1,000 for western blotting; 1:600 and 1:200 for immunofluorescence with Tau(1–368) and APP^{C586} antibodies, respectively). The FSH-blocking polyclonal antibody (FSH-Ab) and humanized monoclonal antibody (Hu6) were generated by Genscript, and developed and characterized in the Zaidi laboratory^{5,21}. siFsh (sc-35415) was obtained from Santa Cruz, and the TUNEL In Situ Cell Death Detection Kit (11684817910) was obtained from Roche. Human Aβ40 (KHB3481), Aβ42 (KHB3544) and inflammatory cytokine ELISA kits (BMS224-2 and KHC0061) were purchased from Invitrogen. The human FSH ELISA kit was obtained from Abcam (ab108641). The mouse FSH (CSB-E06871m-96) and LH ELISA (CSB-E12770m-96) kits were from Cusabio. The 17-β estradiol ELISA kit was obtained from Abcam (ab108667). The AEP substrate Z-Ala-Ala-Asn-AMC (4033201) was obtained from Bachem, and the EZ-Link Sulfo-NHS-LC-Biotinylation Kit was obtained from Thermo Fisher Scientific (21435). Recombinant human FSH used in vitro and in vivo experiments was obtained from Sigma-Aldrich (F4021) and EastCoast Bio (LA252), respectively. The 90-day-release pellets containing 0.36 mg 17-β-estradiol (NE121) were purchased from Innovative Research of America. All chemicals not mentioned above were purchased from Sigma-Aldrich.

Human tissue

Post-mortem brain tissue for western blotting and PCR was obtained from the Emory Alzheimer's Disease Research Center and was approved both by the Biospecimen Committee (approved on 10 February 2021, renewal 1 April 2022), and the Institutional Review Board (IRB) (approved on 12 February 2019; IRB00045782). For ViewRNA studies, we used a flash-frozen, never-thawed brain sample from a 85-year-old white male (de-identified) from Mount Sinai's NIH Brain Tissue Repository (NBTR) (IRB Exempt Status: HS#:13-00709 PS).

Human brain transcriptomics analysis using ViewRNA

We used two AD-vulnerable regions—the hippocampus and para-hippocampal cortex. Serial, cryostat sections (thickness, 12 µm) in the coronal plane were treated with proteinase K followed by in situ hybridization and amplification with specific probe sets in combination: *FSHR-T6* and *MALAT1-T1* using the QuantiGene ViewRNA Assay

Article

(Invitrogen). The sections were counterstained with Gill's hematoxylin. This enabled us to map the cellular expression of *Fshr* in *MALAT1*-positive neurons. Images were acquired using our Zeiss Axio-Imager Z1 and Pannoramic 250 (3DHistech) high-resolution scanner.

Quantitative mouse brain transcriptomics by RNAscope

RNAscope allowed the detection of single transcripts in wild type mouse brain. In brief, 20 pairs of double-Z probes specific to the *Fshr* transcript (ACD Biotech, 400468) were used to hybridize sections. Preamplifiers were allowed to hybridize to the 28 bp binding site formed by each double-Z probe. The amplifiers then further bound to the multiple binding sites on each preamplifier and, finally, labelled probes containing a chromogenic molecule were allowed to bind to multiple sites of each amplifier. Brain tissue and testes were collected from wild-type and *Fshr*^{-/-} male mice. In brief, mice were anaesthetized with isoflurane (2–3% in oxygen; Baxter Healthcare) and perfused transcardially with 0.9% heparinized saline followed by 4% paraformaldehyde (PFA). Brains and testes were extracted, sectioned into 0.5-cm-thick slices and post-fixed in 4% PFA for 12 h before being transferred to 70% ethanol for 24 h, and embedded in paraffin after gradual ethanol dehydration. Coronal sections were cut at 5 µm. For brain, every tenth section was mounted onto ~20 slides, with two sections on each slide. This method enabled us to cover all regions of the brain and to eliminate the likelihood of counting the same transcript twice. Sections were stored at –80 °C. RNAscope was performed using the ACD RNAscope HD Brown LS Reagent Kit and RNAscope LS 2.5 Probe for Mm-*Fshr*. The slides were thawed at room temperature for 10 min before baking at 60 °C for 60 min. The slides were deparaffinized, air-dried for 5 min, blocked with hydrogen peroxide for 10 min at room temperature and pretreated using Target Retrieval Solution at 100 °C for 20 min and Protease Plus at 40 °C for 30 min. Probe hybridization and signal amplification were performed according to the manufacturer's instructions for chromogenic assays. The slides were imaged on an Aperio CS2 Scanner (Leica) and CaseViewer v.2.4 (3DHistech). The Allen Mouse Brain Atlas (<https://mouse.brain-map.org/static/atlas>) was used to identify and manually map *Fshr*-positive cells with precision at each neuroanatomical level. Thereafter, transcripts were counted under high magnification (×40) in each relevant region and subregion (shown in Fig. 2e).

Cells

The human neuroblastoma cell line SH-SY5Y was obtained from ATCC and was not authenticated or tested for mycoplasma contamination. SH-SY5Y was cultured in DMEM/F12 with 10% fetal bovine serum (v/v), penicillin (100 U ml⁻¹, w/v) and streptomycin (100 µg ml⁻¹, w/v). SH-SY5Y transfection was performed using Lipofectamine 3000 (Invitrogen). Primary culture of rat cortical neurons was described previously⁵³. AAV2-siFshrvirus (iAAV05724202) was purchased from Applied Biological Materials. LV-shCebpb-GFP, LV-GFP and AAV-AEP^{C189S} were packaged by the Viral Vector Core (VVC) of Emory University. Neurons cultured 7 days in vitro (DIV 7) were transfected with LV-shCebpb-GFP, LV-GFP, AAV-AEP^{C189S} or AAV2-siFshrvirus. Virus solution (2 µl) was added to 1 ml culture medium and applied to primary neuron cultures. Seven days later (DIV 14), the neurons were treated with FSH (30 ng ml⁻¹) for 48 h. The cells were incubated at 37 °C in a humidified atmosphere of 5% CO₂.

AEP activity assay

Tissue homogenates or cell lysates (10 µg) were incubated in 200 µl assay buffer (20 mM citric acid, 60 mM Na₂HPO₄, 1 mM EDTA, 0.1% CHAPS and 1 mM dithiothreitol, pH 6.0) containing 20 µM δ-secretase substrate, Z-Ala-Ala-Asn-AMC (Bachem). AMC released by substrate cleavage was quantified by measuring at 460 nm using a fluorescence plate reader at 37 °C in kinetic mode.

qPCR analysis

mRNA levels were analysed using qPCR. In brief, RNA was isolated by TRIzol (Life Technologies). Reverse transcription was performed

using SuperScript III reverse transcriptase (Life Technologies). Gene-specific primers and Taqman probes were designed and bought from Applied Biosystems (human *GAPDH* (Hs02758991), mouse *Gapdh* (Mm99999915), rat *Gapdh* (Rn01775763); human *CEPB* (Hs00942496), mouse *Cebpb* (Mm00843434); human *LGNN* (Hs00271599), mouse *Lgmn* (Mm01325350); human *APP* (Hs00169098), mouse *App* (Mm01344172); human *MAPT* (Hs00902194), mouse *Mapt* (Mm00521988); and human *FSHR* (Hs01019695), mouse *Fshr* (Mm00442819) and rat *Fshr* (Rn01648507). All qPCR reactions were performed using the ABI 7500-Fast Real-Time PCR System (SDS v.2.3) and the Taqman Universal Master Mix Kit (Life Technologies). The relative quantification of gene expression was calculated using the ΔΔC_t method.

Western immunoblotting

Cells and brain tissue were washed with ice-cold PBS and lysed in 50 mM Tris-HCl, pH 7.4, 40 mM NaCl, 1 mM EDTA, 0.5% Triton X-100, 1.5 mM Na₃VO₄, 50 mM NaF, 10 mM sodium pyrophosphate and 10 mM sodium β-glycerophosphate, supplemented with protease inhibitor cocktail at 4 °C for 0.5 h, and centrifuged for 25 min at 15,000 rpm. The supernatant was boiled in SDS loading buffer. After SDS-PAGE, the samples were transferred to a nitrocellulose membrane. The membrane was blocked with TBS containing 5% non-fat milk and 0.1% Tween 20 (TBST) at room temperature for 2 h, followed by incubation with primary antibodies at 4 °C overnight, and with secondary antibodies at room temperature for 2 h (the dilutions are described in the 'Antibodies and reagents' section). After washing with TBST, the membrane was developed using the enhanced chemiluminescent detection system.

Immunostaining

We use free-floating 25 µm brain sections for immunostaining. For immunohistochemistry, brain sections were treated with 0.3% H₂O₂ (v/v) for 10 min. The sections were washed three times in PBS and blocked in 1% BSA (w/v) and 0.3% Triton X-100 (v/v) for 30 min, followed by overnight incubation with anti-Aβ (1:400) and anti-AT8 (1:200) antibodies at 4 °C. The signal was developed using the Mouse and Rabbit Specific HRP/DAB (ABC) Detection IHC kit (Abcam). For immunofluorescence staining, sections were incubated overnight at 4 °C with primary anti-Aβ (1:400), anti-APP(C586) (1:200), anti-AT8 (1:200) or anti-Tau(1–368) (1:600) antibodies. After washing with Tris-buffered saline, the sections were incubated with a mixture of labelled secondary antibodies for detection. Details of antibody combinations are provided in the Reporting Summary. DAPI (1 µg ml⁻¹) (Sigma-Aldrich) was used for staining nuclei. For thioflavin-S and Aβ double staining, slides were first stained with anti-Aβ antibodies, rinsed in PBS and then stained with freshly prepared 0.0125% thioflavin-S in 50% ethanol for 10 min. The sections were washed with 50% ethanol and placed in distilled water. Images were acquired with an Olympus Confocal FV1000 Imaging System.

Gallyas silver staining

Brain sections (25 µm) were incubated in 5% periodic acid for 5 min, washed in water and then placed in alkaline silver iodide solution (containing 1% (v/v) silver nitrate) for 1 min. The sections were then washed in 0.5% acetic acid (v/v) for 10 min, placed in developer solution for 15 min, and washed with 0.5% acetic acid (v/v) and then with water. The sections were treated with 0.1% gold chloride for 5 min, washed in water and incubated in 1% sodium thiosulfate (v/v) for 5 min before a final washing.

Golgi staining

Mouse brains were fixed in 10% formalin (v/v) for 24 h and then immersed in 3% potassium bichromate (w/v) for 3 days in the dark. The solution was changed each day and the brains were transferred

into 2% silver nitrate (w/v) solution and incubated for 7 days in the dark. The solution was changed each day. Vibratome sections were cut at 30 µm, air dried for 10 min, dehydrated through 95% and 100% ethanol, cleared in xylene and coverslips were applied. Spine numbers were counted as described previously⁵⁴.

Transmission electron microscopy of synapses

After deep anaesthesia, mice were perfused transcardially with 4% paraformaldehyde (v/v) in PBS. Hippocampal slices were post-fixed in cold 1% OsO₄ (w/v) for 1 h. Samples were prepared and examined using standard procedures. Ultrathin sections (90 nm) were stained with uranyl acetate and lead acetate and viewed at 100 kV under a JEOL 200CX Electron Microscope. Synapses were identified by the presence of synaptic vesicles and postsynaptic densities. Synapse number was quantified as described previously^{25,26}.

Morris water maze

Mice were trained in a round, water-filled tub (diameter, 52 inches) in an environment rich with extra maze cues, as described previously. Each subject was given 4 trials per day for 5 consecutive days with a 15 min intertrial interval. The maximum trial length was 60 s and, if mice did not reach the platform in the allotted time, they were manually guided to it. After the 5 days of task acquisition, a probe trial was presented during which time the platform was removed and the percentage of time spent in the quadrant that previously contained the escape platform during task acquisition was measured over 60 s. All trials were analysed for latency by means of MazeScan (TopScan v.3.0, Clever Sys).

Novel-object recognition test

Mice were presented with two identical objects during the first session, and then one of the two objects was replaced by a novel object during a second session⁵⁵. On day 1, a habituation phase in an empty arena (for 5 min), was followed 24 h later by the training phase, which allows for a 5 min exploration in the habituated arena in which two identical objects are placed in opposite quadrants. The testing phase followed a gap of 20 min. For testing, one object was replaced with a novel object followed by 5 min of exploration. Data were collected using the ANY-maze Video Tracking System v.3.3 (Stoelting).

Electrophysiology

Mice were anaesthetized with isoflurane, decapitated and their brains were dropped in ice-cold artificial cerebrospinal fluid (a-CSF) containing 124 mM NaCl, 3 mM KCl, 1.25 mM NaH₂PO₄, 6.0 mM MgCl₂, 26 mM NaHCO₃, 2.0 mM CaCl₂ and 10 mM glucose. Hippocampi were dissected and cut into 400-µm-thick transverse slices with a vibratome. After incubation at 23–24 °C in a-CSF for 60–90 min, the slices were placed in a recording chamber (RC-22C, Warner Instruments) on the stage of an upright microscope (Olympus CX-31) and perfused at a rate of 3 ml per min with a-CSF (containing 1 mM MgCl₂) at 23–24 °C. A 0.1 MΩ tungsten monopolar electrode was used to stimulate the Schaffer collaterals. fEPSPs were recorded under current-clamp mode in CA1 stratum radiatum by a glass microelectrode filled with a-CSF with a resistance of 3–4 MΩ. The stimulation output (Master-8; AMPI) was controlled by the trigger function of an EPC9 amplifier (HEKA Elektronik). Data were filtered at 3 kHz and digitized at sampling rates of 20 kHz using PatchMaster v.2x90.1 (HEKA Elektronik). Stimulus intensity (0.1 ms duration, 10–30 mA) was set to evoke 40% of the maximum fEPSP and the test pulse was applied at a rate of 0.033 Hz. The LTP of fEPSPs was induced by 3 theta-burst-stimulation (4 pulses at 100 Hz, repeated 3 times with a 200 ms interval). The magnitudes of LTP are expressed as the mean percentage of the baseline fEPSP initial slope.

Distribution studies

The fluorescent signal following the injection of AlexaFluor750-tagged FSH or Hu6 was quantified in dissected tissues using the IVIS Spectrum

In Vivo Imaging System (Perkin Elmer). For ⁸⁹Zr-distribution studies, a solution of ⁸⁹Zr oxalate in 1 M oxalic acid was neutralized using a 1 M Na₂CO₃ solution until a pH of 6.8–7.4 was reached. The ⁸⁹Zr solution was added to the DFO-containing Hu6 and incubated at 37 °C using a thermomixer (600 rpm) for 60 min. The resulting solution was purified using a PD-10 column with PBS as eluent. C57BL/6 mice were injected with ⁸⁹Zr-DFO-Hu6 (100 µCi) through the tail vein. The mice were imaged by PET, and were euthanized after extensive perfusion with PBS (24–48 h after injection). Brains were collected and weighed before counting radioactivity on a 2480 Wizard² automatic γ-counter (Perkin Elmer). Radioactivity data were corrected for decay and normalized to tissue weight to express radioactivity concentration as the percentage injected dose per gram.

Statistical analysis

Statistical analyses were performed using GraphPad Prism v.8. The tests were either unpaired two-tailed Student's *t*-test (two-group comparison) or one-way ANOVA followed by Fisher's least significant difference post hoc test (more than two groups). Differences with *P* < 0.05 were considered to be significant. *P* values are annotated in the figures and extended data figures, and are provided in the source data.

Ensuring rigour and reproducibility

There is a nascent movement to ensure that preclinical data is true and accurate^{56–61}. M.Z. and C.J.R. coined the phrase 'contemporaneous reproducibility,' which refers to the synchronous reproduction of data in more than one laboratory. As Zaidi's discovery of the effects of FSH on body fat were new and unexpected, he reached out to C.J.R. for help in the form of a reproducibility study. Key datasets were reproduced by C.J.R. in a process that lasted for more than three years, as other validation studies were added by both laboratories. The term replicability refers to the ability of one or more independent groups to replicate a finding using a different technology or method—replicability is a measure of truth or significance of a given finding²⁹. Here we replicated the key finding, namely the effect of the FSH-Ab, in the K.Y. and M.Z. laboratories using two mouse models of AD and separate protocols to examine FSH-Ab action in both sexes. We have also used three transcriptomic technologies, qPCR (M.Z. laboratory), RNAscope (Alamak Biosciences) and ViewRNA (V.H. laboratory) to reproduce the findings on *FSHR* expression in the mouse and human brain. To further enhance rigour and transparency, we have exchanged Excel spreadsheets to cross-check primary datasets and reviewed each figure independently to determine accuracy. Everything from simple immunoblots to microscopy images has been vetted by the research groups. Such validation practices, we believe, require unfettered transparency and remain fundamental to ensuring rigour.

Ensuring integrity of microscopy images

Images were visualized by the three independent observers in several steps (V.R., T.Y. and V.M.). First, raw camera images were loaded onto a Cloud by S.S.K. Second, individual images were downloaded and scrutinized against the corresponding panel in the manuscript to ensure that the published images matched the source dataset. Third, we compared merged immunofluorescence images against their original single images to be certain that the merge arose from the specific single images. Fourth, we overexposed or dimmed the background to verify the integrity of both single and merged images. Fifth, to make sure that there were no accidental duplications, we compared each image against all other images in the manuscript. Finally, during the latter test, we also rotated and flipped each image to validate integrity.

Reporting summary

Further information on research design is available in the Nature Research Reporting Summary linked to this paper.

Data availability

All original western blots are provided in the Supplementary Information. The original unedited camera images for histology and immunohistochemistry are available online (<https://osf.io/9hp8r/>). There are no restrictions on data availability. Unique biological material will be made available to other investigators on request. Source data are provided with this paper.

51. Sterneck, E., Tessarollo, L. & Johnson, P. F. An essential role for C/EBP β in female reproduction. *Genes Dev.* **11**, 2153–2162 (1997).
52. Minkeviciene, R. et al. Amyloid β -induced neuronal hyperexcitability triggers progressive epilepsy. *J. Neurosci.* **29**, 3453–3462 (2009).
53. Zhang, Z. et al. 7,8-dihydroxyflavone prevents synaptic loss and memory deficits in a mouse model of Alzheimer's disease. *Neuropsychopharmacology* **39**, 638–650 (2014).
54. Xiang, J. et al. Delta-secretase-cleaved Tau antagonizes TrkB neurotrophic signalings, mediating Alzheimer's disease pathologies. *Proc. Natl Acad. Sci. USA* **116**, 9094–9102 (2019).
55. Leger, M. et al. Object recognition test in mice. *Nat. Protoc.* **8**, 2531–2537 (2013).
56. Ioannidis, J. P. Why most published research findings are false. *PLoS Med.* **2**, e124 (2005).
57. Collins, F. S. & Tabak, L. A. Policy: NIH plans to enhance reproducibility. *Nature* **505**, 612–613 (2014).
58. McNutt, M. Reproducibility. *Science* **343**, 229 (2014).
59. Mullard, A. Cancer reproducibility project yields first results. *Nat. Rev. Drug Discov.* **16**, 77 (2017).
60. Horrigan, S. K. et al. Replication study: melanoma genome sequencing reveals frequent PREX2 mutations. *eLife* **6**, e21634 (2017).
61. Horrigan, S. K., Reproducibility Project: Cancer Biology. Replication study: the CD47-signal regulatory protein alpha (SIRPa) interaction is a therapeutic target for human solid tumors. *eLife* **6**, e18173 (2017).

Acknowledgements This work performed at Emory University School of Medicine was supported by NIH grants RF1 AG051538 and R01 AG065177 to K.Y. K.Y. thanks the staff at the Alzheimer's Disease Research Center at Emory University for human samples; the Rodent Behavioral Core (RBC), one of the Emory Integrated Core Facilities; the Viral Vector Core of the Emory Neuroscience NINDS Core Facility (P30 NS055077); and the NIH's Georgia Clinical and Translational Science Alliance (UL1 TR002378). Work at Icahn School of Medicine at Mount Sinai performed at the Center for Translational Medicine and Pharmacology (CeTMaP) was supported by U19 AG060917 to M.Z. and C.J.R.; R01 DK113627 to M.Z. and J.I.; and R01

AG071870, R01 AG074092 and U01 AG073148 to T.Y. and M.Z. M.Z. thanks the Harrington Discovery Institute for the Innovator-Scholar Award towards development of the FSH-Ab. C.J.R. acknowledges support from the NIH (P20 GM121301 to C.J.R.). We thank M. Ehrlich and S. Gandy for their intellectual contributions, and S. Babunovic for proofreading the final version of the paper.

Author contributions K.Y. conceived the idea that FSH may be a mediator of AD in post-menopausal women and, together with M.Z., jointly proposed that blocking FSH using M.Z.'s polyclonal FSH-Ab could prevent AD. Thereafter, V.R., M.Z. and T.Y. designed the experiments, analysed the data and jointly wrote the manuscript. J.X., S.S.K. and Z.W. designed and performed most of the experiments and analysed the data. X.L. prepared primary neurons and assisted with mouse experiments. P.C. performed RNAscope studies. V.R. and A.G. recorded and analysed RNAscope data. F.K., J.B. and S.M. conducted studies with APP/PS1 mice for contemporaneous replication^{6,29}. K.I. and D.L. performed the *Fshr* mRNA expression studies. D.S., A.P. and S.G. generated FSH-Ab and Hu6. T.-C.K. and S.G. performed antibody distribution studies. P.K. and V.H. conceived and performed the ViewRNA studies with human brain. S.-P.Y. and Z.Z. assisted with data analysis and interpretation. In summary, K.Y.'s laboratory was primarily responsible for generating data in Figs. 1a–e, 2a–c, f, 3, 4 and 5 and Extended Data Figs. 1a–e, 2a–c, f and 3–10. M.Z.'s laboratory produced data in Figs. 1f and 2d–e, g and Extended Data Fig. 1i–p. Moreover, J.I., K.A.G. and C.J.R. assisted with the conception of experiments and manuscript preparation. T.Y., V.M. and V.R. checked image integrity with the help of J.X., S.S.K. and K.Y.; A.G. and T.F. edited and revised the manuscript. T.-C.K. rechecked the raw data files. T.Y., V.R., M.Z. and K.Y. oversaw overall data management and provenance.

Competing interests M.Z. is listed as an inventor on issued patents on inhibiting FSH for the prevention and treatment of osteoporosis and obesity: US patent numbers 5,436,285 (1995, awarded to Icahn School of Medicine at Mount Sinai (ISMMS)), 5,674,887 (1997, awarded to ISMMS and University of Pittsburgh), 8,435,948 (2013, awarded to ISMMS) and 11,034,761 (2021, awarded to ISMMS). M.Z. is also listed as an inventor on a pending patent application on composition and use of humanized monoclonal anti-FSH antibodies. These patents are owned by ISMMS, and M.Z. would be recipient of royalties according to institutional policy. M.Z. and K.Y. are listed as inventors of a pending patent application on the use of FSH as a target for preventing Alzheimer's disease. The latter patent is jointly owned by ISMMS and Emory University, and M.Z. and K.Y. would be recipient of royalties according to institutional policy. The other authors declare no competing interests.

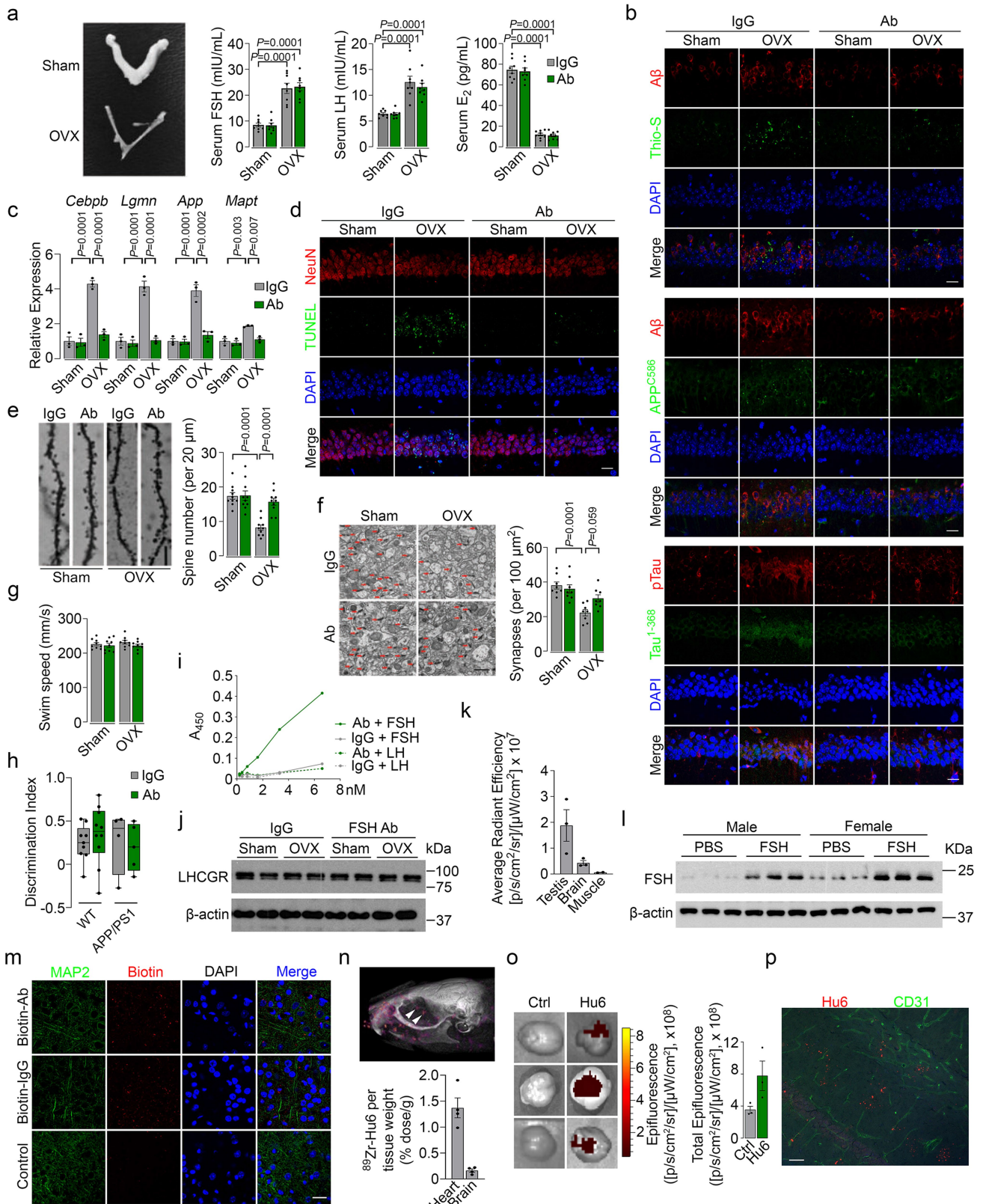
Additional information

Supplementary information The online version contains supplementary material available at <https://doi.org/10.1038/s41586-022-04463-0>.

Correspondence and requests for materials should be addressed to Mone Zaidi or Keqiang Ye.

Peer review information *Nature* thanks Li Gan and the other, anonymous, reviewer(s) for their contribution to the peer review of this work.

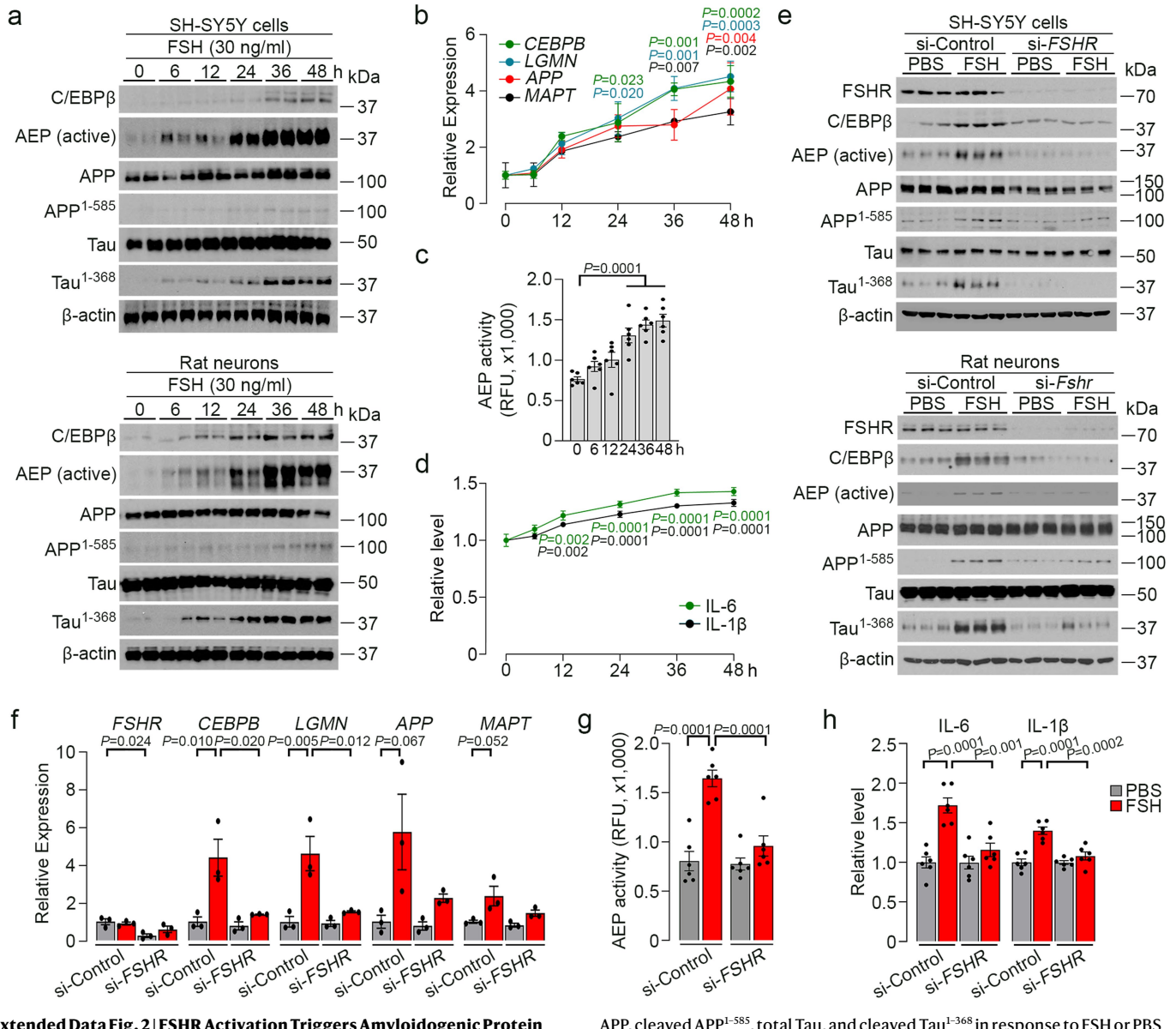
Reprints and permissions information is available at <http://www.nature.com/reprints>.



Extended Data Fig. 1 | See next page for caption.

Article

Extended Data Fig. 1 | Effects of Anti-FSH β Antibody in Reversing Ovariectomy-Induced Neuropathology in 3xTg Mice. **a**, Ovariectomized 3xTg mice displayed hypoplastic thread-like uteri and elevated serum FSH and LH levels. FSH-Ab (200 μ g/mouse, every 2 days, i.p., 8 weeks) did not alter total serum FSH, LH or 17 β -estradiol levels. Statistics: mean \pm s.e.m., N = 8 mice per group, one-way ANOVA. **b**, Immunofluorescent micrographs showing enhanced labelling in the following pairs: amyloid β (A β , red) and thioflavin-S (Thio-S, green); A β (red) and cleaved APP C586 (green); and pTau (red) and Tau $^{1-368}$ (green) in the hippocampus after OVX, and its amelioration with FSH-Ab (scale bar, 20 μ m). **c**, Upregulation of *Cebpb*, *Lgmn*, *App* and *Mapt* in OVX mouse brains, with reversal to near-baseline with FSH-Ab. Statistics: mean \pm s.e.m., N = 3 mice per group, one-way AVOVA. **d**, Immunofluorescence micrographs showing that OVX induces apoptosis (TUNEL, green) in hippocampal NeuN-positive neurons (red); this apoptosis is abolished by FSH-Ab (scale bar, 20 μ m). **e**, Golgi staining on brain sections from CA1 region post-OVX shows a substantial reduction in spine numbers, which is corrected with the FSH-Ab (scale bar, 5 μ m). Statistics: mean \pm s.e.m., N = 3 mice per group (10 sections), one-way AVOVA. **f**, Transmission electron micrographic images and quantitative analysis of synapses in hippocampal sections post-OVX treated with IgG or FSH-Ab (scale bar, 1 μ m). Statistics: mean \pm s.e.m., N = 3 mice per group (8 sections), one-way AVOVA. **g**, Morris Water Maze testing shows no differences in swim speed. Statistics: mean \pm s.e.m., N = 9 mice per group, one-way ANOVA. **h**, Cognitive testing using the Novel Object Recognition test revealed the absence of significant difference between *APP/PS1* and non-transgenic mice in Discrimination Index [(Novel Object Head Entry – Familiar Object Head Entry)/Total Head Entry]; the result is expected at 9 months of age in *APP/PS1* mice. Thus, no effect of FSH-Ab was noted at this age, despite the reduction in A β 40 and A β 42 accumulation shown in Fig. 1f. Statistics: mean \pm s.e.m., mice per group 9, 10, 4 and 4 from left to right; Whisker plot, upper and lower ends of the whiskers show maxima and minima, line in box shows median, and upper and lower box boundaries show 75th and 25th percentile, respectively; unpaired two-tailed Student's *t*-test; **i**, ELISA showing no cross-reactivity of FSH-Ab with LH. **j**, Western immunoblot showing no change in expression of the LHCGR in whole brain lysates upon OVX or FSH-Ab treatment (N = 2 mice per group). **k**, IVIS imaging of isolated tissues from mice injected with AlexaFluor750-FSH, i.v., showing localization of FSH in the brain (N = 3 mice per group). **l**, Western immunoblots of whole brain lysates showing that i.p. injection of human FSH (5 IU) causes an elevation of brain FSH (N = 3 mice per group). **m**, Immunofluorescence micrographs showing the detection of peripherally injected (i.p.) biotinylated FSH-Ab (red) and biotinylated goat IgG (red) in brain sections (scale bar, 20 μ m). Note the absence of cellular or nuclear co-localization with MAP2 or DAPI, respectively. **n**, Representative PET image shows that ^{89}Zr -labelled humanized monoclonal FSH-Ab (^{89}Zr -Hu6), injected i.v., is localized to live brain (arrows). γ -counting in perfused tissue shows presence of ^{89}Zr -Hu6 in dissected brain tissue at 24 and 48 h post-injection (N = 4 mice). **o**, IVIS imaging and quantitation with AlexaFluor750-labelled Hu6, given i.v. shows localization in perfused whole brain tissue; N = 3 mice per group. Control (Ctrl): phosphate-buffered saline (PBS). **p**, Confirmatory immunofluorescence on the same mice (**o**) using anti-human IgG showing Hu6 localization (red) in proximity to CD31 $^+$ endothelial cells (green) (scale bar, 100 μ m). For gel source data, see Supplementary Fig. 1.

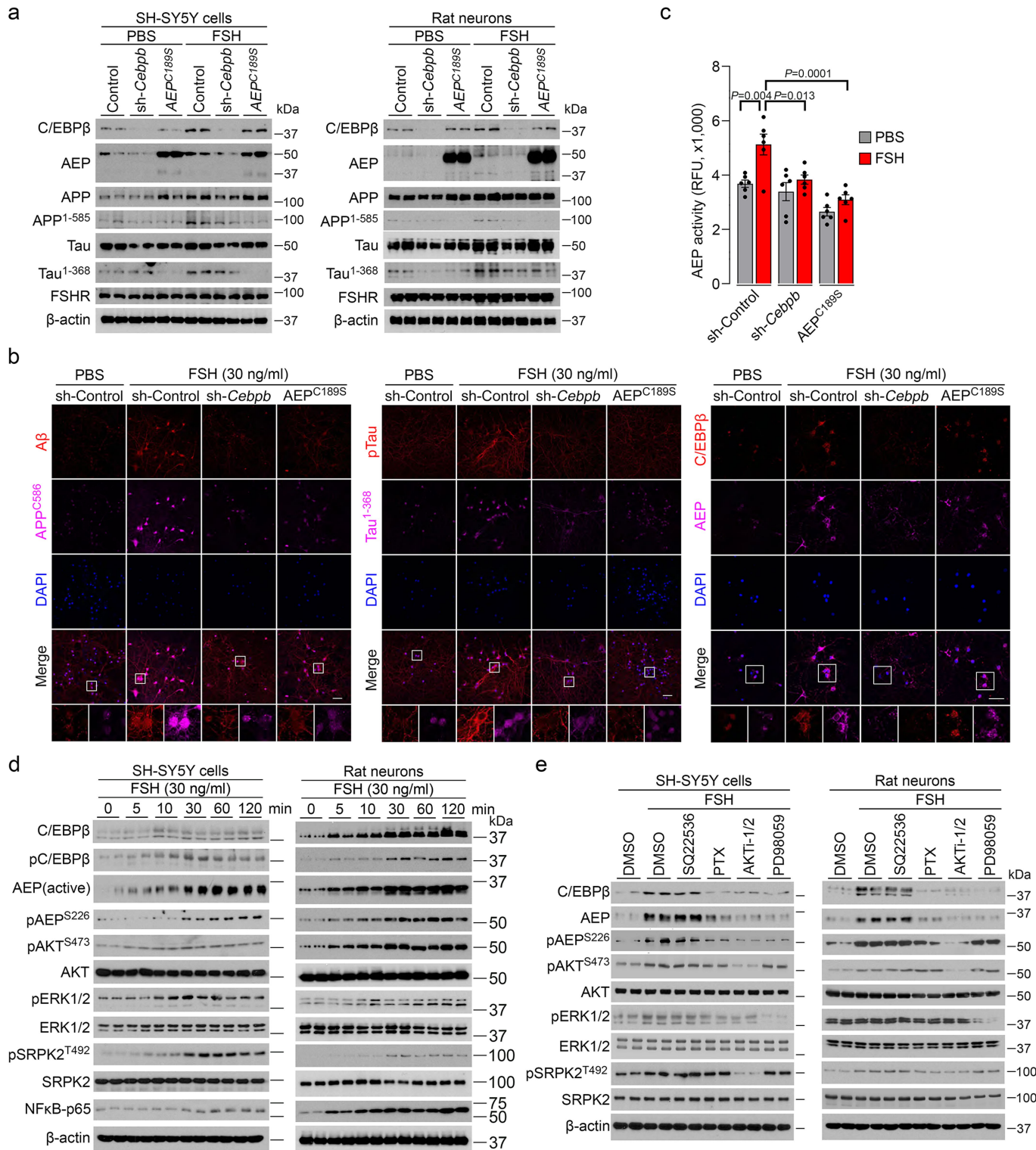


Extended Data Fig. 2 | FSHR Activation Triggers Amyloidogenic Protein Accumulation.

a, Western immunoblots showing the effect of activating neuronal FSHRs by FSH (30 ng/mL) in human SH-SY5Y and primary rat neuronal cells on the expression of C/EBP β , AEP, as well as the cleavage of amyloid precursor protein (APP) and Tau using antibodies noted in ‘Methods’. FSH (30 ng/mL) likewise stimulated the expression of CEBPB, LGMN, APP and MAPT (qPCR) (**b**); AEP activity (**c**); and certain inflammatory cytokines (ELISA), namely IL-6 and IL-1 β (**d**). Statistics: mean \pm s.e.m.; Mice per group, (**b**) 3, (**c**) 6, and (**d**) 6; one-way ANOVA. **e**, Western immunoblotting showing C/EBP β , AEP,

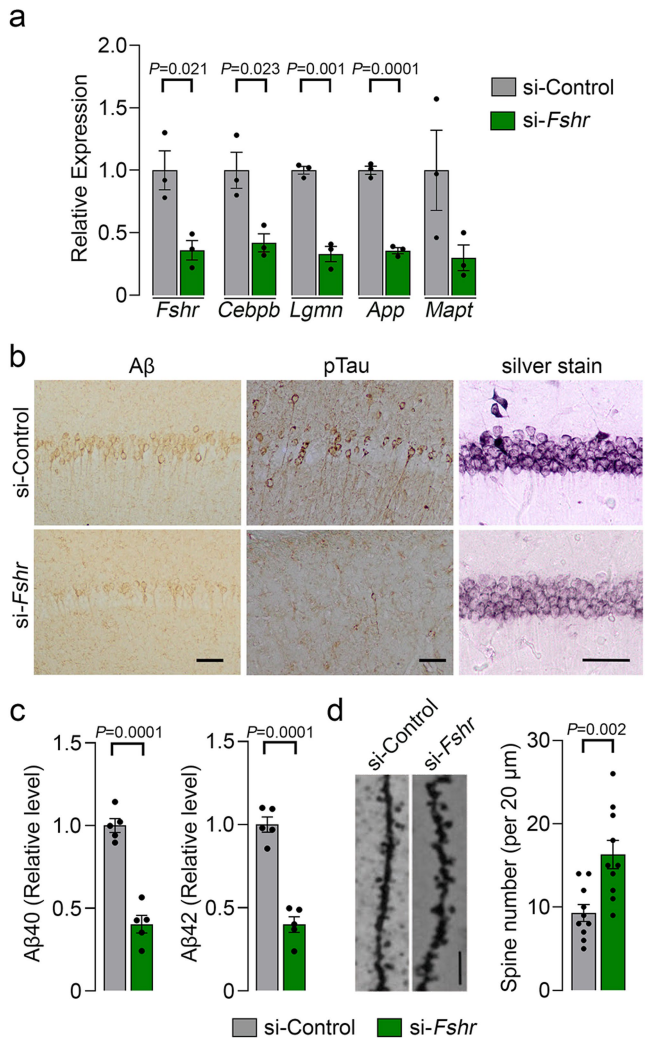
APP, cleaved APP $^{1-585}$, total Tau, and cleaved Tau $^{1-368}$ in response to FSH or PBS following transfection with human FSHR siRNA (si-FSHR) for SH-SY5Y cells or rat Fshr siRNA (si-Fsh) for primary rat neurons, or appropriate scrambled siRNAs. **f**, mRNA levels of CEBPB, LGMN, APP and MAPT in SH-SY5Y cells incubated with FSH after control or si-FSHR transfection. **g**, AEP activity after incubation with FSH in control or si-FSHR-transfected SH-SY5Y cells. **h**, IL-6 and IL-1 β levels (ELISAs) in SH-SY5Y cells incubated with FSH following control or si-FSHR infection. Statistics: mean \pm s.e.m.; (**f**) 3 biological replicates; (**g**, **h**) 6 mice per group; one-way ANOVA.

Article



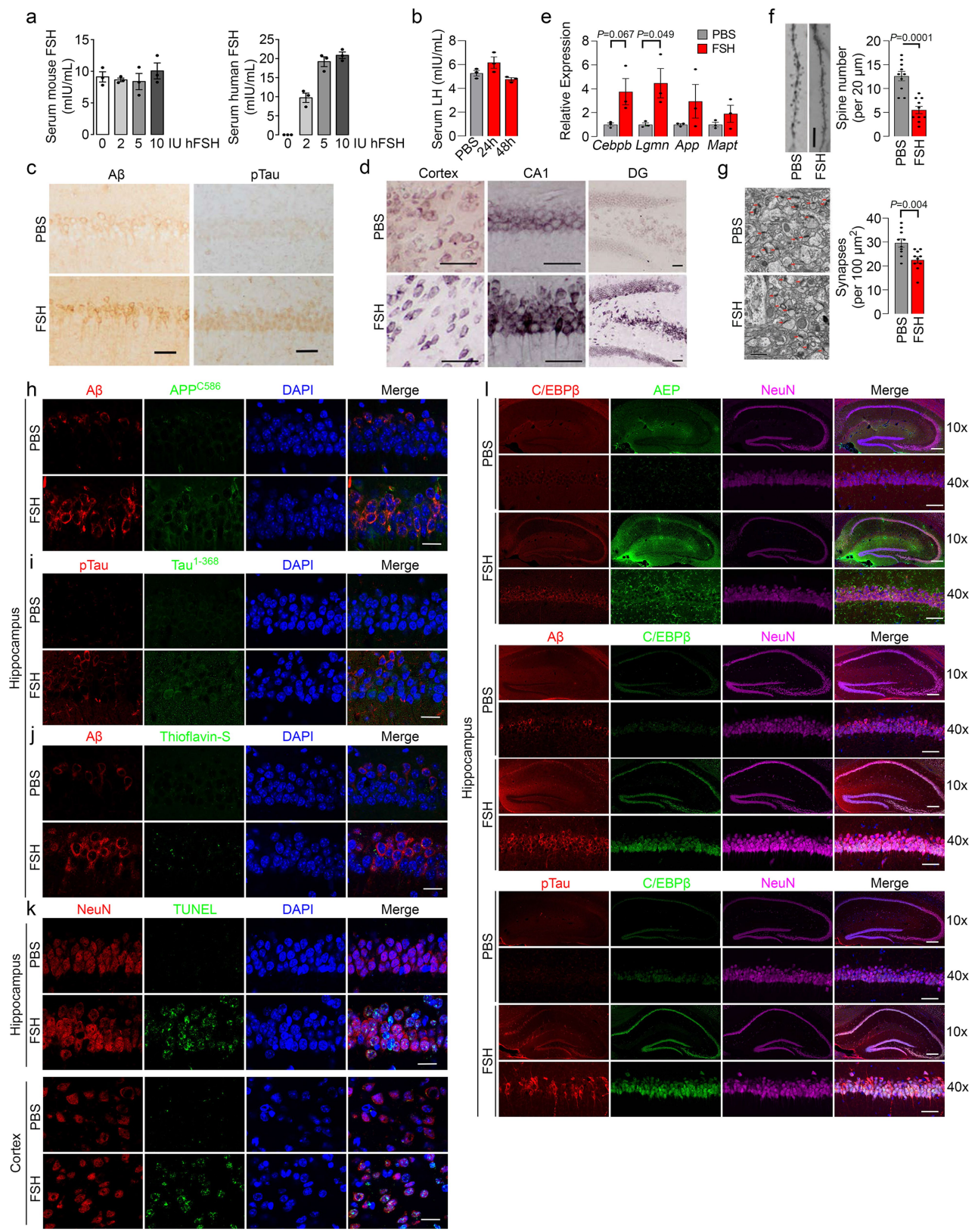
Extended Data Fig. 3 | FSH Induces APP and Tau Cleavage Through C/EBP β and AEP/6-Secretase Activation in Human SH-SY5Y Cells and Rat Cortical Neurons. **a**, Western immunoblots showing the effect of FSH (30 ng/mL) on Tau, APP, AEP and FSHR of knocking down C/EBP β expression by lentiviral infection with shRNA-Cebpb (sh-Cebpb) or reducing 6-secretase activity by adeno-associated virus infection of AEP $C189S$ in both human SH-SY5Y cells and rat cortical neurons. The stimulatory action of FSH was reversed at 48 h. **b, c**, Effect of FSH (30 ng/mL) on APP, APP C586 , pTau and Tau $^{1-368}$ accumulation (immunofluorescence, scale bar, 40 μ m, **b**) and AEP activity (**c**) in rat cortical neurons infected with sh-Cebpb or AAV-AEP $C189S$. Statistics: (**c**) mean \pm s.e.m.;

$N = 6$ mice per group; one-way ANOVA. **d**, Western immunoblots showing the time course of FSH effects on C/EBP β , phosphorylated C/EBP β (pC/EBP β), AEP, pAEP S^{226} , total AKT, pAKT S^{473} , total ERK1/2, pERK1/2, total SRPK2, pSRPK2 T^{492} and pNF κ B-p65. **e**, Western immunoblots showing the effect of a 30-minute incubation with FSH (30 ng/mL) on levels of C/EBP β , AEP, pAEP S^{226} , total AKT and pAKT S^{473} , total ERK1/2 and pERK1/2, total SRPK2 and pSRPK2 T^{492} in the presence or absence of the cAMP inhibitor SQ22536 (100 μ M), G α_i inhibitor pertussis toxin (PTX, 50 ng/ml), AKTi-1/2 inhibitor (10 μ M) and ERK1/2 inhibitor PD98059 (10 μ M).



Extended Data Fig. 4 | Targeted Knockdown of *Fshr* in the Hippocampus Diminishes AD Pathologies. **a**, Quantitative PCR shows significantly reduced expression of *Fshr*, *Cebpb*, *Lgmn*, *App* and *Mapt*. **b**, Immunohistochemistry of the hippocampus shows reduced accumulation of A β and pTau, as well as of proteinaceous deposits (silver staining) in si-*Fshr*-injected OVX mice (scale bar, 50 μ m). **c**, The two isoforms of A β , namely A β 40 and A β 42, were also reduced. **d**, Notable is the marked increase in dendritic spines (Golgi staining) (scale bar, 5 μ m). Statistics: mean \pm s.e.m., (a) 3 biological replicates; (c) 5 mice per group; (d) 10 sections from 3 mice per group; unpaired two-tailed Student's *t*-test.

Article

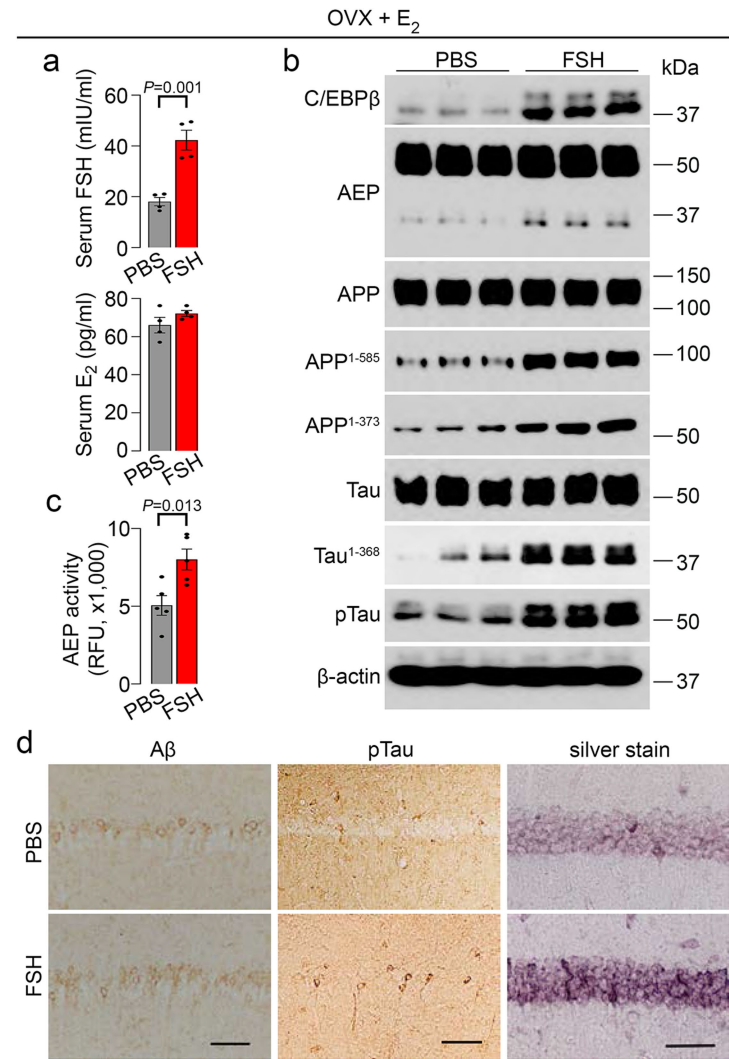


Extended Data Fig. 5 | See next page for caption.

Extended Data Fig. 5 | Recombinant FSH Triggers AD Pathology in 3xTg Mice.

a, Serum FSH levels—both mouse (endogenous) and human (exogenous)—24 h after i.p. injection of 2, 5 or 10 IU human recombinant FSH. **b**, Serum LH levels also shown. Female 3xTg mice were injected with recombinant FSH (5 IU per mouse, daily, i.p., 3 months). **c**, Immunohistochemistry for A β or pTau in hippocampus post-FSH injection (scale bar, 50 μ m). **d**, Silver staining of the prefrontal cortex, and hippocampal CA1 and dentate gyrus (DG) regions showing enhanced proteinaceous deposits in FSH-injected mice (scale bar, 50 μ m). **e**, Brain mRNA levels of *Cebpb*, *Lgmn*, *App* and *Mapt*. **f**, Golgi staining of brain sections from the CA1 region shows reduced spine numbers in FSH-injected mice (scale bar, 5 μ m).

g, Transmission electron micrographs of hippocampal sections showing reduced synapse numbers post-FSH (scale bar, 1 μ m). Immunofluorescence micrographs showing the following image pairs in the hippocampus and/or cortex post-FSH: **(h)** A β (red) and cleaved APP C586 (green); **(i)** pTau (red) and cleaved Tau $^{1-368}$ (green); **(j)** A β (red) and thioflavin-S (green); and **(k)** NeuN (red) and TUNEL (green) (scale bar, 20 μ m). **l**, Immunofluorescence showing co-localization of C/EBP β , AEP, A β and pTau to NeuN-positive neurons upon FSH stimulation [10x (scale bar, 300 μ m) and 40x (scale bar, 50 μ m) magnifications]. Statistics: mean \pm s.e.m., **(a, b)** 3 mice per group; **(e)** 3 biological replicates, **(f, g)** 10 sections from 3 mice per group; unpaired two-tailed Student's *t*-test.

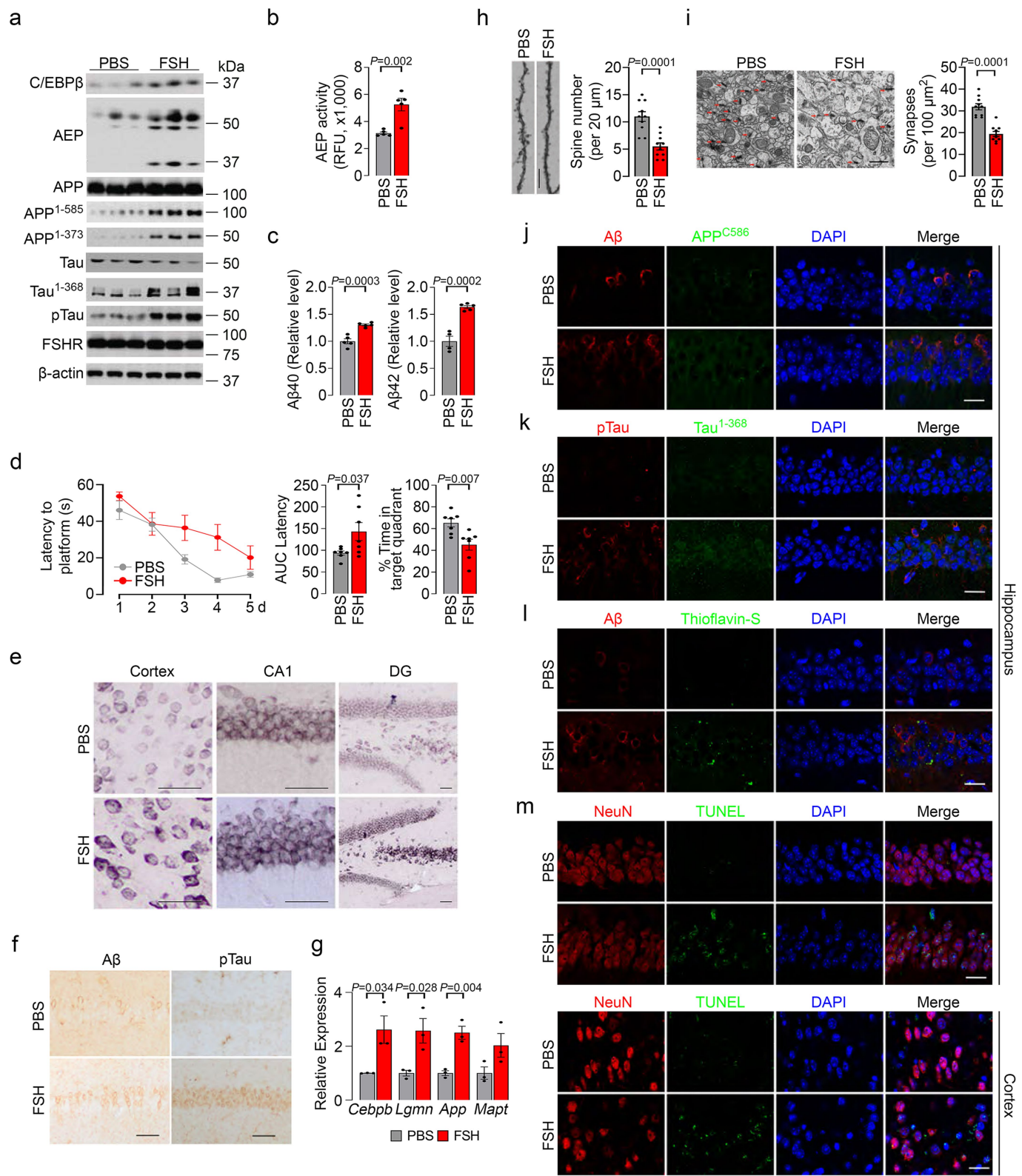


Extended Data Fig. 6 | Effect of Recombinant FSH in Triggering AD Pathology in Ovariectomized 3xTg Mice With Oestrogen Replacement.

3xTg mice were ovariectomized at 3 months and supplemented with 17 β -estradiol using 90-day-release pellets (E2, 0.36 mg) to render them biochemically eugonadal. The mice were randomly divided to be injected with PBS or recombinant human FSH (5 IU per mouse, daily, i.p., 3 months). **a**, Serum level of FSH and 17 β -estradiol. **b**, Western immunoblotting showing increased

C/EBP β , AEP, cleaved APP¹⁻³⁷³ and APP¹⁻⁵⁸⁵, total Tau, cleaved Tau¹⁻³⁶⁸ and pTau in the brain after FSH injection. **c**, Brain AEP enzymatic activity also shown.

d, Immunohistochemistry of the hippocampus shows increased expression of A β and pTau in the FSH group. Silver staining showed increased proteinaceous deposits in FSH-treated mice (scale bar, 50 μ m). Statistics: mean \pm s.e.m., mice per group; (**a**) 4 and (**c**) 5; unpaired two-tailed Student's *t*-test.



Extended Data Fig. 7 | See next page for caption.

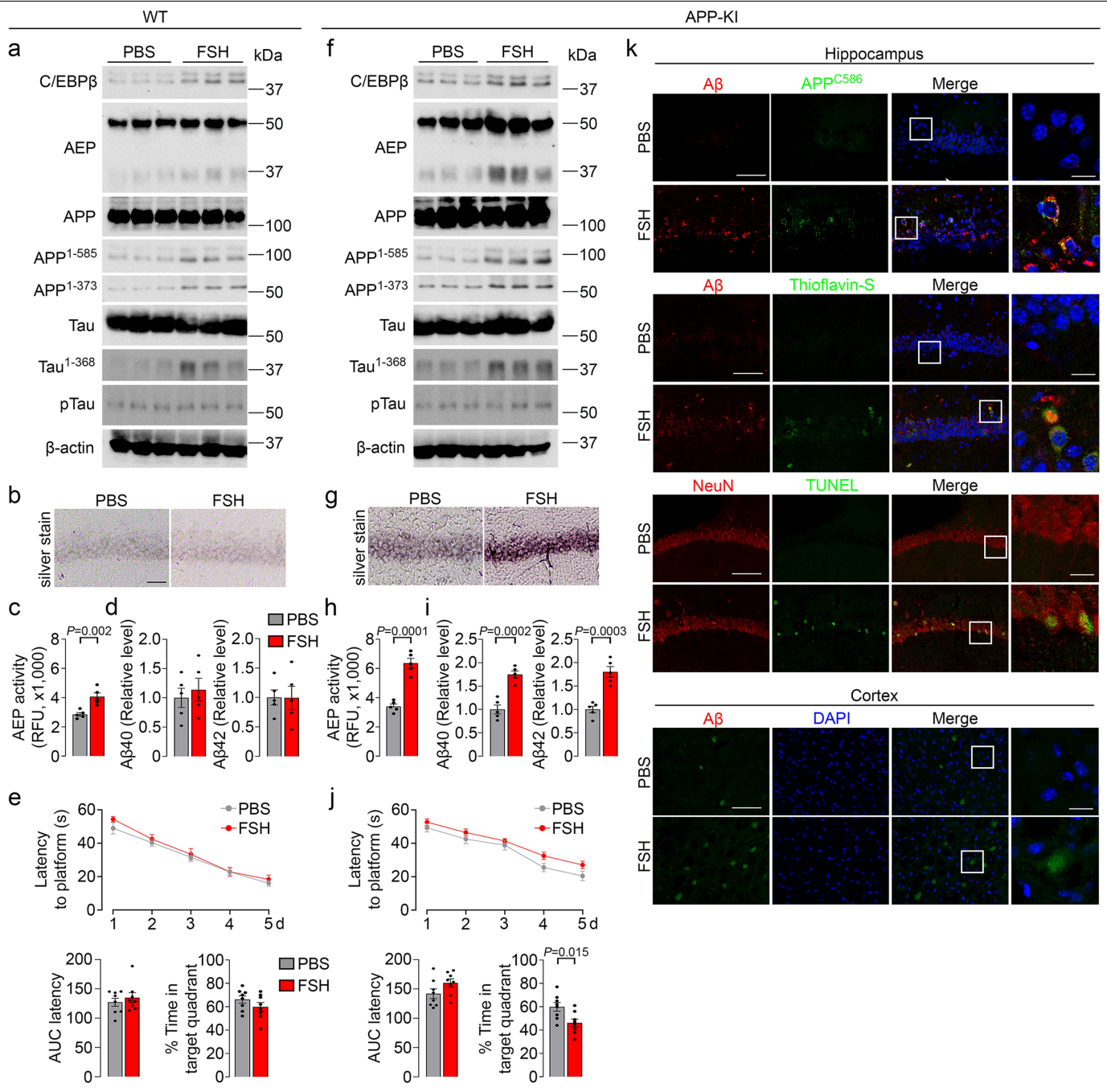
Article

Extended Data Fig. 7 | Effect of Recombinant FSH in Triggering AD

Pathology and Cognitive Decline in Male Mice. Male 3xTg mice were injected with recombinant FSH at 5 IU per mouse daily, i.p. for 3 months. **a**, Western immunoblots showing increased C/EBP β , AEP, cleaved APP $^{1-373}$ and APP $^{1-585}$, total Tau, cleaved Tau $^{1-368}$ and pTau in the brain (3 mice per group). **b, c**, Brain AEP activity (**b**) and A β isoforms, A β 40 and A β 42 (**c**) were also increased with FSH. **d**, Morris Water Maze test shows enhanced escape latency to mount the platform (seconds). Also shown are integrated escape latency (area under the curve, AUC) and percentage of time spent in the target quadrant (Probe Trial Test). **e**, Silver staining of the prefrontal cortex, and hippocampus CA1 and dentate gyrus (DG) regions showing enhanced proteinaceous deposits in FSH-injected mice (scale bar, 50 μ m). **f**, Immunohistochemistry for A β or pTau in the

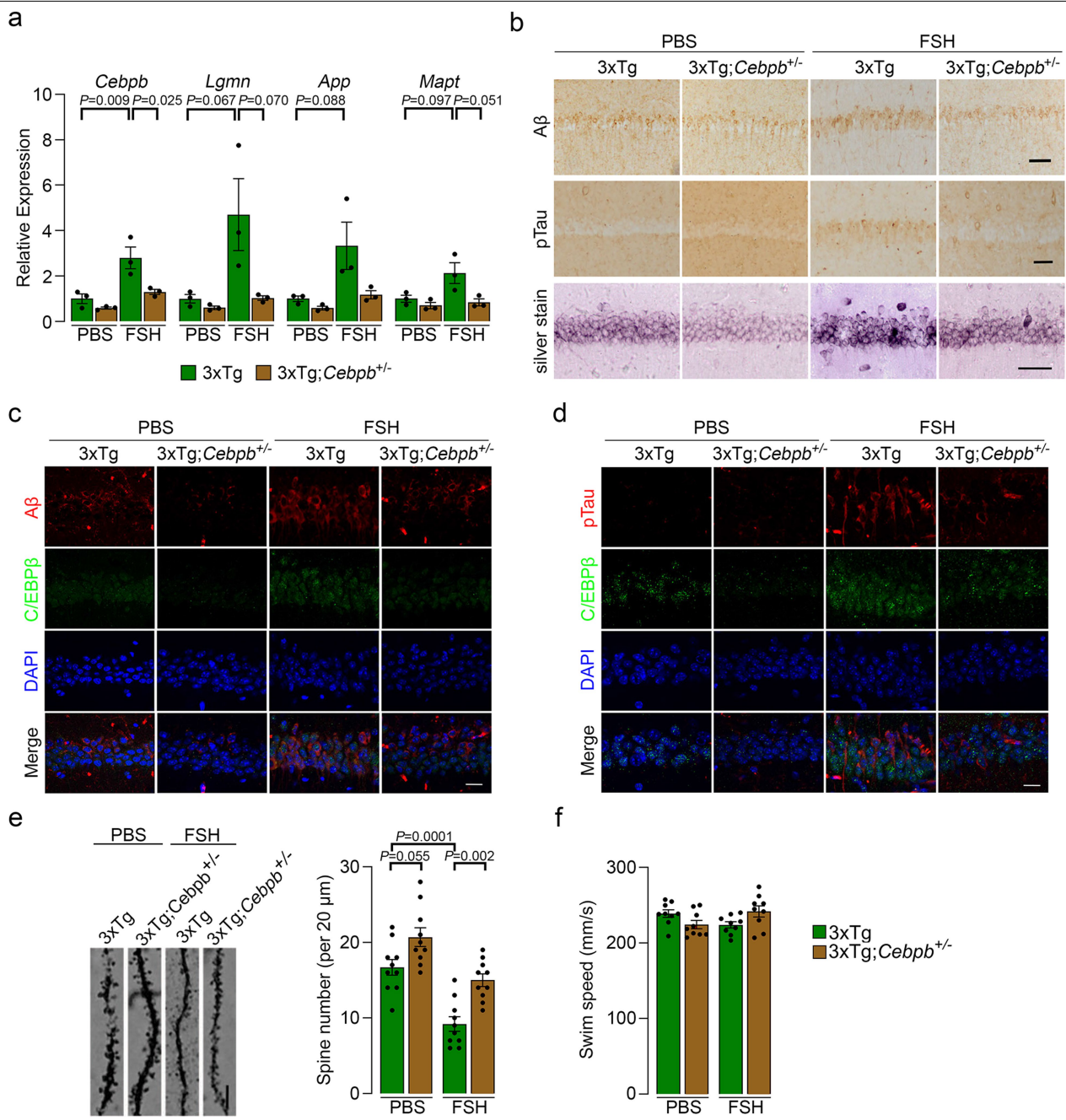
hippocampus post-FSH injection (scale bar, 50 μ m). **g**, Brain mRNA levels of *Cebpb*, *Lgmn*, *App* and *Mapt*. **h**, Golgi staining of brain sections from the CA1 region of the hippocampus showing reduced spine numbers in FSH-injected mice (scale bar, 5 μ m). **i**, Transmission electron micrographs of hippocampal sections showing reduced synapse numbers post-FSH (scale bar, 1 μ m).

Immunofluorescence micrographs showing the following image pairs: (**j**) A β (red) and cleaved APP C586 (green); (**k**) pTau (red) and cleaved Tau $^{1-368}$ (green); (**l**) A β (red) and thioflavin-S (green); and (**m**) NeuN (red) and TUNEL (green) in the hippocampus and/or cortex of male 3xTg mice after FSH (scale bar, 20 μ m). Statistics: mean \pm s.e.m., mice per group, (**b, c**) 5, (**d**) 7, (**g**) 3, (**h, i**), 3 (10 sections); unpaired two-tailed Student's *t*-test.



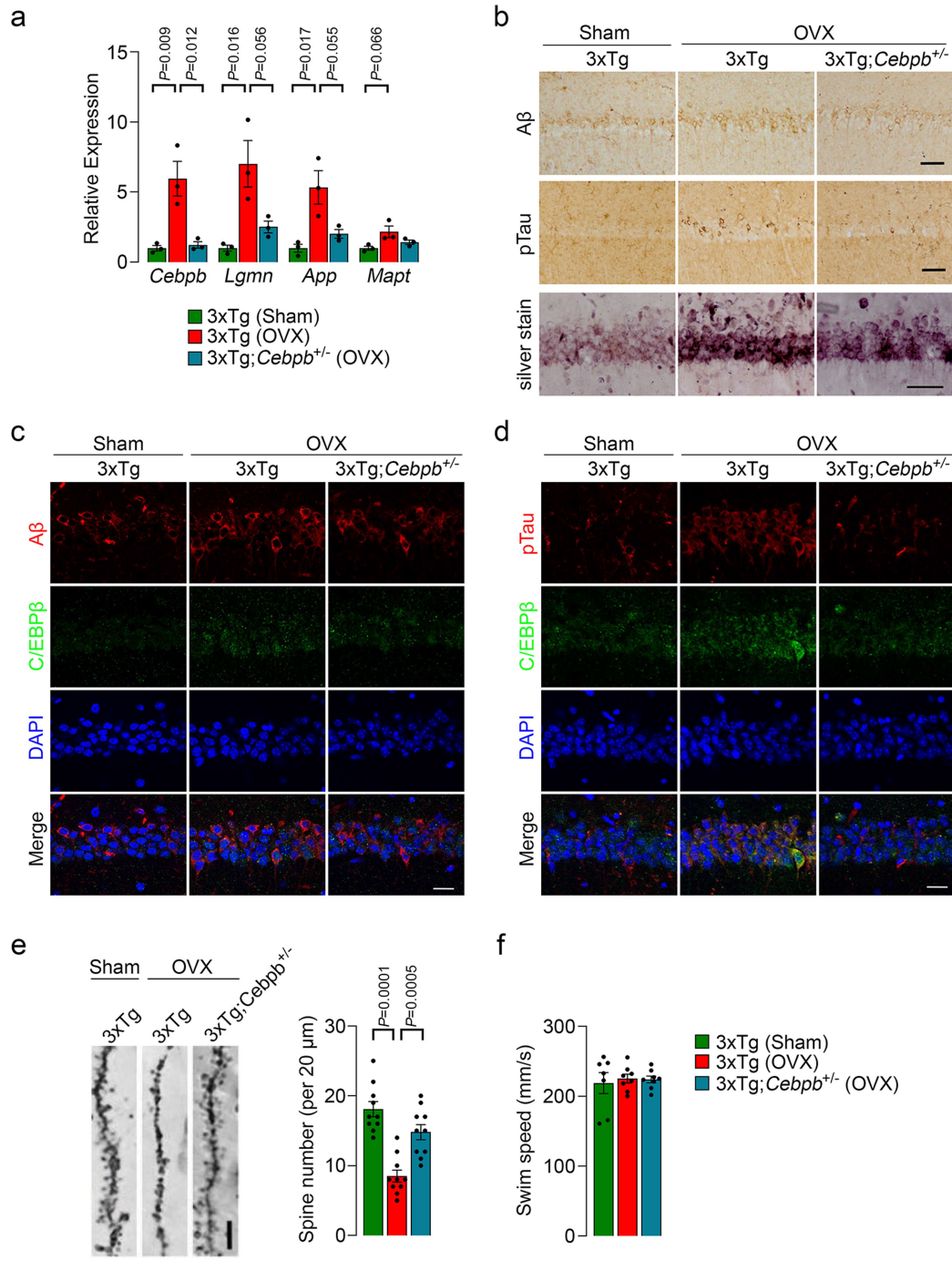
Extended Data Fig. 8 | Effect of FSH in Triggering AD Pathology and Cognitive Decline in Female Wild Type and APP-KI Mice. In APP-KI mice, three amino acid substitutions (G601R;F606Y;R609H) are knocked into A β -coding exon 14 of the APP gene—this results in the non-transgenic expression at basal levels of oligomerizable human A β . Female wild type and APP-KI mice were injected with recombinant FSH (5 IU, daily, i.p. 3 months). **a-d**, In wild type mice, Western immunoblotting showing increased C/EBP β , AEP, cleaved APP $^{1-373}$ and APP $^{1-585}$, total Tau, and cleaved Tau $^{1-368}$ in whole brain (3 mice per group) (**a**), as well as increased silver staining (**b**), elevated AEP activity (**c**) and increases A β isoforms, A β 40 and A β 42 (**d**) upon FSH treatment. **e**, Morris Water Maze test, however, showed no difference in escape latency to mount the platform (seconds). Also shown are no differences in integrated

escape latency (area under the curve, AUC) and percentage of time spent in the target quadrant (Probe Trial Test). **f-i**, Western immunoblotting showing elevations in C/EBP β , AEP, cleaved APP $^{1-373}$ and APP $^{1-585}$, and cleaved Tau $^{1-368}$ in whole brain (**f**), along with enhancements in silver staining (**g**), AEP activity (**h**), and A β isoforms (**i**) in APP-KI mice in response to FSH injection. **j**, There was also a significant spatial memory deficit on the Morris Water Maze test. **k**, Immunofluorescence micrographs showed increases in the hippocampus and/or cortex of female APP-KI mice post-FSH injected in the following pairs: A β (red) and cleaved APP C^{586} (green); A β (red) and thioflavin-S (green); and NeuN (red) and TUNEL (green). Scale bar: (b, g) 50 μ m, (k) 100 μ m (magnified view), 10 μ m). Statistics: mean \pm s.e.m.; mice per group, (**c, d, h, i**) 5, (**e, j**) 8; unpaired two-tailed Student's *t*-test.



Extended Data Fig. 9 | C/EBP β Mediates FSH-Induced AD Neuropathology and Cognitive Decline in 3xTg Mice. **a**, *Cebpb*, *Lgmn*, *App* and *Mapt* mRNA expression following FSH injection to 3xTg or *Cebpb*^{+/-} 3xTg mice. Statistics: mean \pm s.e.m., $N=3$ biological replicates, one-way ANOVA. **b**, Immunohistochemistry for A β and pTau and silver staining for proteinaceous deposits (scale bar, 50 μ m). **c–e**, Immunofluorescence staining for A β (red) and C/EBP β (green) (**c**) and

for pTau (red) and C/EBP β (green) (**d**) (scale bar, 20 μ m), and Golgi staining for dendritic spines (**e**) in the hippocampus in female 3xTg or *Cebpb*^{+/-} 3xTg mice, post-FSH (scale bar, 5 μ m). Statistics: mean \pm s.e.m., 10 sections from 3 mice per group, one-way ANOVA. **f**, Morris Water Maze testing showed no difference in swim speed. Statistics: 9 mice per group, one-way ANOVA.



Extended Data Fig. 10 | C/EBP β Mediates Ovariectomy-Induced AD Neuropathology and Cognitive Decline in 3xTg Mice. **a**, *Cebpb*, *Lgmn*, *App* and *Mapt* mRNA expression following ovariectomy of 3xTg or *Cebpb*^{+/-} 3xTg mice. Statistics: mean \pm s.e.m., 3 biological replicates, one-way ANOVA. **b**, Immunohistochemistry for A β and pTau and silver staining for proteinaceous deposits (scale bar, 50 μ m). **c–e**, Immunofluorescence staining for A β (red) and C/EBP β (green) (c) and for pTau (red) and C/EBP β (green) (d) (scale bar, 20 μ m), and Golgi staining for dendritic spines (e) in the hippocampus in female 3xTg or *Cebpb*^{+/-} 3xTg mice (scale bar, 5 μ m), post-OVX. Statistics: mean \pm s.e.m., 10 sections from 3 mice per group, one-way ANOVA. **f**, Morris Water Maze test showed no difference in the swim speed between 3xTg and *Cebpb*^{+/-} 3xTg mice. Statistics: left to right: 7, 8, 8 mice per group, one-way ANOVA.

C/EBP β (green) (c) and for pTau (red) and C/EBP β (green) (d) (scale bar, 20 μ m), and Golgi staining for dendritic spines (e) in the hippocampus in female 3xTg or *Cebpb*^{+/-} 3xTg mice (scale bar, 5 μ m), post-OVX. Statistics: mean \pm s.e.m., 10 sections from 3 mice per group, one-way ANOVA. **f**, Morris Water Maze test showed no difference in the swim speed between 3xTg and *Cebpb*^{+/-} 3xTg mice. Statistics: left to right: 7, 8, 8 mice per group, one-way ANOVA.

Reporting Summary

Nature Research wishes to improve the reproducibility of the work that we publish. This form provides structure for consistency and transparency in reporting. For further information on Nature Research policies, see our [Editorial Policies](#) and the [Editorial Policy Checklist](#).

Statistics

For all statistical analyses, confirm that the following items are present in the figure legend, table legend, main text, or Methods section.

n/a Confirmed

- The exact sample size (n) for each experimental group/condition, given as a discrete number and unit of measurement
- A statement on whether measurements were taken from distinct samples or whether the same sample was measured repeatedly
- The statistical test(s) used AND whether they are one- or two-sided
Only common tests should be described solely by name; describe more complex techniques in the Methods section.
- A description of all covariates tested
- A description of any assumptions or corrections, such as tests of normality and adjustment for multiple comparisons
- A full description of the statistical parameters including central tendency (e.g. means) or other basic estimates (e.g. regression coefficient) AND variation (e.g. standard deviation) or associated estimates of uncertainty (e.g. confidence intervals)
- For null hypothesis testing, the test statistic (e.g. F , t , r) with confidence intervals, effect sizes, degrees of freedom and P value noted
Give P values as exact values whenever suitable.
- For Bayesian analysis, information on the choice of priors and Markov chain Monte Carlo settings
- For hierarchical and complex designs, identification of the appropriate level for tests and full reporting of outcomes
- Estimates of effect sizes (e.g. Cohen's d , Pearson's r), indicating how they were calculated

Our web collection on [statistics for biologists](#) contains articles on many of the points above.

Software and code

Policy information about [availability of computer code](#)

Data collection For Morris Water Maze and Novel Object Recognition tests, the data were captured and analyzed by MazeScan (Clever Sys, Inc.) and ANY-maze Video Tracking System (Stoelting, UK, version 3.3), respectively. For quantitative PCR, we used the ABI 7500 SDS Software Version v2.3. Electrophysiology data were analyzed by PatchMaster software ver. 2x90.1 (HEKA Elektronik). CaseViewer (3D Histech, Budapest, Hungary, version 2.4) was used to visualize mouse RNAscope data.

Data analysis Graphpad Prism v.8 was used to analyze the data.

For manuscripts utilizing custom algorithms or software that are central to the research but not yet described in published literature, software must be made available to editors and reviewers. We strongly encourage code deposition in a community repository (e.g. GitHub). See the Nature Research [guidelines for submitting code & software](#) for further information.

Data

Policy information about [availability of data](#)

All manuscripts must include a [data availability statement](#). This statement should provide the following information, where applicable:

- Accession codes, unique identifiers, or web links for publicly available datasets
- A list of figures that have associated raw data
- A description of any restrictions on data availability

All Excel files and original Western blots are provided on the Nature website. The original unedited camera images for histology and immunohistochemistry are available at <https://osf.io/9hp8r/>. There are no restrictions on data availability. In addition, unique biological material will be made available to other investigators upon request, as is customary. The Allen Mouse Brain Atlas was used to identify brain regions and sub-regions (<https://mouse.brain-map.org/static/atlas>).

Field-specific reporting

Please select the one below that is the best fit for your research. If you are not sure, read the appropriate sections before making your selection.

Life sciences Behavioural & social sciences Ecological, evolutionary & environmental sciences

For a reference copy of the document with all sections, see nature.com/documents/nr-reporting-summary-flat.pdf

Life sciences study design

All studies must disclose on these points even when the disclosure is negative.

Sample size	No statistical methods were used to calculate sample size. Instead, sample sizes were determined based on previous studies by Dr. Ye's and other groups.
Data exclusions	No data were excluded.
Replication	We have replicated the key finding, namely the effect of the FSH Ab, in the Ye and Zaidi labs using three mouse models of AD and separate protocols to examine reversal versus prevention, respectively, in different sexes. We have also utilized the same technique, qPCR, to reproduce findings on Fshr expression in the brain. In situ hybridization was performed independently in two labs to detect FSHR transcripts in the brain (RNAscope for the mouse brain, and ViewRNA for the human brain). All attempts at replication were successful. To further enhance rigor and transparency, we have exchanged Excel spreadsheets to cross-check primary data sets, and reviewed each figure independently to determine accuracy. Everything from simple immunoblots to in vivo images has been vetted by both research groups. Such validation practices, we believe, require unfettered transparency and remain fundamental to ensuring rigor. Such contemporaneous replication was previously achieved by us in Liu et al. (Nature, 2017) [PMID: 28538730]. The process is documented in Rosen and Zaidi (2017) [PMID: 28810084].
Randomization	Mice were randomly selected to be assigned into separate groups--namely, ovariectomy or sham-operation, PBS or FSH, IgG or FSH Ab, and si-control or si-Fshr.
Blinding	Key behavioral studies at Emory University were conducted in the Rodent Behavioral Core by technicians who were unaware of the mouse groups. Data collection and analyses were automated for objective measurements, namely ELISA, qPCR, AEP enzymatic activity, and LTP studies. Findings were consistent between the automated objective measures and more subjective measurements, such as immunohistochemistry, histology, and Western blotting, within the same experiment. Distribution studies simply showed label in the brain.

Reporting for specific materials, systems and methods

We require information from authors about some types of materials, experimental systems and methods used in many studies. Here, indicate whether each material, system or method listed is relevant to your study. If you are not sure if a list item applies to your research, read the appropriate section before selecting a response.

Materials & experimental systems		Methods	
n/a	Involved in the study	n/a	Involved in the study
<input type="checkbox"/>	<input checked="" type="checkbox"/> Antibodies	<input checked="" type="checkbox"/>	<input type="checkbox"/> ChIP-seq
<input type="checkbox"/>	<input checked="" type="checkbox"/> Eukaryotic cell lines	<input checked="" type="checkbox"/>	<input type="checkbox"/> Flow cytometry
<input checked="" type="checkbox"/>	<input type="checkbox"/> Palaeontology and archaeology	<input checked="" type="checkbox"/>	<input type="checkbox"/> MRI-based neuroimaging
<input type="checkbox"/>	<input checked="" type="checkbox"/> Animals and other organisms		
<input type="checkbox"/>	<input checked="" type="checkbox"/> Human research participants		
<input checked="" type="checkbox"/>	<input type="checkbox"/> Clinical data		
<input checked="" type="checkbox"/>	<input type="checkbox"/> Dual use research of concern		

Antibodies

Antibodies used	Antibodies to C/EBP β (mouse monoclonal, catalog#: sc-7962, clone H-7), C/EBP β (rabbit polyclonal, catalog#: sc-150) and FSH β (mouse monoclonal, catalog #: SC-374452, clone C12) were from Santa Cruz; anti-AEP 6E3 (Millipore, mouse monoclonal, catalog#: MABN2304, clone 6E3) was a gift from Dr. Colin Watts, Professor of Immunobiology, Division of Cell Signaling and Immunology, College of Life Sciences, University of Dundee, Dundee, UK; antibodies to FSHR (rabbit polyclonal, catalog#: PA5-50963), pTauS202,T205 (mouse monoclonal, AT8, catalog#: MN1020) and IBA1 (goat polyclonal, catalog# PA5-18039) were from Thermo Fisher Scientific; antibodies to Legumain (a.k.a. AEP) (rabbit monoclonal, catalog#: 93627, clone D6S4H), AKT (rabbit monoclonal, catalog#: 4691s, clone # C67E7), pAKTS473 (rabbit polyclonal, catalog#: 9271s), ERK1/2 (rabbit polyclonal, catalog#: 9102s), pERK1/2 (Thr202/Tyr204, mouse monoclonal, catalog#: 9106s, clone E10) were purchased from Cell Signaling Technology; antibody to NeuN (mouse monoclonal, catalog#: MAB377, clone A60), NeuN (guinea pig polyclonal, catalog# ABN90), Tau (210-241, mouse monoclonal, catalog#: MAB361, clone tau-5), β -actin (mouse monoclonal, catalog#: A5316, clone AC-74) and GFAP (mouse monoclonal, catalog# MAB360, clone GA5) were from Sigma-Aldrich; antibody to A β (mouse monoclonal, catalog#: 800701, clone 4G8) was obtained from Biogelend; and antibody to SRPK2 (mouse monoclonal, catalog#: 611118, clone 23/SRK2) was from BD
-----------------	--

Biosciences. Rabbit polyclonal antibodies to pAEPS226, Tau1-368, APP1-585, APP1-373, APPC586 and pSRPK2T492 were developed in the Ye lab. AlexaFluor488- and 594-coupled secondary antibodies were: goat anti-mouse IgG (H+L) cross-adsorbed secondary antibody, Alexa Fluor 488, Invitrogen, A11001, Lot 2220848; goat anti-rabbit IgG (H+L) highly cross-adsorbed secondary antibody, Alexa Fluor 488, Invitrogen, A11034, Lot 2069632; goat anti-Mouse IgG (H+L) cross-adsorbed secondary antibody, Alexa Fluor 594, Invitrogen, A11005, Lot 2179228; goat anti-rabbit IgG (H+L) highly cross-adsorbed secondary antibody, cyanine5, Invitrogen, A10524, Lot 2063326; goat anti-rabbit IgG (H+L) cross-adsorbed secondary antibody, cyanine5, Invitrogen, A10523, Lot 2156245; goat anti-guinea pig IgG antibody, pre-adsorbed (Cy5), GeneTex, GTX26567, Lot 25935; donkey anti-goat IgG (H+L) cross-adsorbed secondary antibody, Alexa Fluor 488, Invitrogen, A11055, Lot 2059218. The anti-FSH β polyclonal antibody (FSH Ab) and humanized monoclonal antibody (clone Hu6) were developed and characterized in the Zaidi lab.

Validation

(1) C/EBP β (H-7) detects C/EBP β of mouse, rat and human origin by Western blotting, immunoprecipitation, immunofluorescence and immunohistochemistry. Another C/EBP β antibody (rabbit polyclonal, catalog#: sc-150) has been validated (PMID: 28088614). (2) Anti-AEP 6E3 (Millipore, MABN2304, clone 6E3) detects mouse and human LGMN by Western blotting, immunoprecipitation, immunofluorescence and immunohistochemistry [PMID: 12860980]. (3) Antibody to FSHR (polyclonal, catalog#: PA5-50963) has been validated for Western blotting, immunofluorescence and ELISA on human, mouse and rat samples. (4) pTauS202,T205 (AT8, catalog#: MN1020) targets PHF-tau (Ser202/Thr205) in ELISA, immunofluorescence, immunohistochemistry, and Western blot applications and shows reactivity with human samples. (5) Antibody to Legumain (catalog#: 93627, clone D6S4H) interacts with human, mouse and rat proteins on immunofluorescence and Western blotting (PMID: 31793911). (6) Antibody to AKT (catalog#: 4691s, clone # C67E7) detects endogenous levels of human, mouse, rat and monkey total Akt protein, and does not cross react with other related proteins by Western blotting, immunofluorescence and other immune detection methods. (7) The pAKTS473 (catalog#: 9271s) antibody detects endogenous levels of human, mouse, rat, hamster, monkey, cow and dog Akt1 only when phosphorylated at Ser473 (Western blotting and immunofluorescence). This antibody also recognizes Akt2 and Akt3 when phosphorylated at the corresponding residues, and does not recognize Akt phosphorylated at other sites, nor does it recognize phosphorylated forms of related kinases such as PKC or p70 S6 kinase. (8) The ERK1/2 (catalog#: 9102s) antibody has been validated for Western blotting and immunohistochemistry of human, mouse, rat, hamster, monkey, mink, cow and pig total p44/42 MAP kinase (Erk1/Erk2) protein. In some cell types, this antibody recognizes p44 MAPK more readily than p42 MAPK. The antibody does not recognize either JNK/SAPK or p38 MAP kinase. (9) Antibody to pERK1/2 (catalog#: 9106s, clone E10) detects human, mouse, rat, hamster, monkey, mink, cow and pig p44 and p42 MAP kinases (Erk1 and Erk2) by Western blotting, when dually phosphorylated at Thr202 and Tyr204 of Erk1 (Thr185 and Tyr187 of Erk2), but not singly phosphorylated at Thr202 or Tyr204. The antibody does not cross-react with the corresponding phosphorylated residues of either SAPK/JNK or p38 MAP kinase. This antibody may cross-react with an unknown cytoskeletal protein in some cell lines as visualized by immunofluorescence. (10) Antibody to NeuN (catalog#: MAB377, clone A60) recognizes neuron-specific NeuN, which is present in most neuronal cell types of all vertebrates, including neurons of cerebellum, cerebral cortex, hippocampus, thalamus, spinal cord and neurons in the peripheral nervous system including dorsal root ganglia, sympathetic chain ganglia and enteric ganglia. (11) Antibody to Tau (210-241, catalog#: MAB361, clone tau-5) detects protein from rat, human and cow and is used for Western blotting. (12) Antibody to β -actin (catalog#: A5316, clone AC-74) detects protein on Western blotting, immunofluorescence and immunohistochemistry in tissues from humans, rat, mouse, pig, dog, and sheep and guinea pig. (12) Antibody to A β (catalog#: 800701, clone 4G8) is reactive to human and mouse β amyloid (amino acid residues 17-24), as well as detects precursor forms, and is used for immunohistochemistry and immunofluorescence. (13) Antibody to SRPK2 (catalog#: 611118, clone 23/SRPK2) detects SRPK2 by Western blotting and immunofluorescence in mouse, human, rat, and dog. (14) Antibody to FSH β (mouse monoclonal, catalog #: SC-374452, clone C12) is recommended for detection of mouse, rat and human FSH β by Western blotting, immunofluorescence and ELISA. (15) Antibody to GFAP (mouse monoclonal, catalog# MAB360, clone GA5) has been validated for use in immunofluorescence and Western blotting for the detection of human, mouse, rat, rabbit, cow and pig GFAP protein in more than 65 citations. (16) Antibody to IBA1 (catalog# PA5-18039) was validated for Western blotting, immunohistochemistry and immunofluorescence in human, mouse and rat tissue. (17) Antibodies to pAEPS226, Tau1-368, APP1-585, APP1-373, APPC586 and pSRPK2T492 were developed in the Ye lab and have been validated in multiple publications for Western blotting, immunohistochemistry and immunofluorescence of human, mouse and rat tissues [PMID: 28826672; PMID: 25326800; PMID: 26549211; and PMID: 19592491]. (18) The polyclonal antibody to the 13-amino-acid-long FSHR-binding epitope of mouse FSH was generated in the goat and validated functionally in the Zaidi lab [PMID: 22908268 and 28538730]. The humanized monoclonal antibody, clone Hu6, has been published in Gera et al., 2020 [PMID: 33127753].

Eukaryotic cell lines

Policy information about [cell lines](#)

Cell line source(s)	SH-SY5Y (ATCC)
Authentication	Not authenticated.
Mycoplasma contamination	Not tested for Mycoplasma.
Commonly misidentified lines (See ICLAC register)	None.

Animals and other organisms

Policy information about [studies involving animals; ARRIVE guidelines](#) recommended for reporting animal research

Laboratory animals	Female (2.5 to 4 month-old) 3xTg mice were obtained from Jackson Laboratory (stock #34830). Male APP/PS1 mice (5 month-old) on a C57BL/6 background were generated and bred at Mount Sinai. APP-KI mice were purchased from Jackson Laboratory (stock #30898). Cebpb $^{+/-}$ mice were originally obtained from Dr. Peter F. Johnson from NIH. These mice were developed in his group and reported in PMID: 9303532. Cebpb mice were maintained at Emory University as heterozygotes on C57BL/6 and 129Sv backgrounds. The two strains were crossed to generate viable F1 hybrid wild type and Cebpb $^{+/-}$ littermates; the latter were then crossed with 3xTg mice to generate compound 3xTg;Cebpb $^{+/-}$ and 3xTg;Cebpb $^{+/-}$ mutants. 3-month-old female mice were used. At both institutions,
--------------------	--

mice were kept under specific pathogen-free conditions in an environmentally-controlled clean room with the humidity range of 40% to 60% and housed at 22 °C on a 12-h/12-h light/dark cycle. Food and water were provided ad libitum.

Wild animals

The study did not involve wild animals.

Field-collected samples

The study did not involve samples to be collected from the field.

Ethics oversight

Animal care and handling were performed according to NIH animal care guidelines at both Emory and Mount Sinai. The protocols were reviewed and approved by the respective Institutional Animal Care and Use Committees

Note that full information on the approval of the study protocol must also be provided in the manuscript.

Human research participants

Policy information about [studies involving human research participants](#)

Population characteristics

Post-mortem brain tissue for Western blotting and PCR was obtained from the Emory Alzheimer's Disease Research Center. For ViewRNA studies, we used a flash-frozen, never-thawed brain specimen from a 85-year-old white male (de-identified) from Mount Sinai's NIH Brain Tissue Repository (NBTR).

Recruitment

The samples for Western blotting or PCR were randomly picked from archives. These samples were not used for comparative studies; instead just to document FSHR in brain. We did not expect male or female differences in FSHR expression or their alteration in disease states.

Ethics oversight

Study at Emory was approved both by the Biospecimen Committee (approved on 02/10/2021, renewal 04/01/2022), and the Institutional Review Board (IRB) (approved on 2/12/2019; IRB#: IRB00045782). Study at Mount Sinai was IRB-exempt (IRB Exempt Status: HS#:13-00709 PS).

Note that full information on the approval of the study protocol must also be provided in the manuscript.